The Application of Experimental Microdosimetry to Mixed-Field Neutron-Gamma Dosimetry

By

Saad Najm Al-Bayati

A Thesis Submitted in Partial Fulfillment

Of the Requirements for the Degree of

Master of Applied Science

In

Nuclear Engineering

Faculty of Energy Systems and Nuclear Science Program

University of Ontario Institute of Technology

December, 2012

Abstract

Absorbed dose distributions in lineal energy for neutrons and gamma rays were measured by using both a tissue-equivalent walled counter (TEPC) and a graphite-walled low pressure proportional counter (GPC) in the Am-Be neutron source facility at UOIT. A series of measurements were performed with the counters filled with propane-based TE gas (55.1% C_3H_8, 39.5% CO_2 and 5.4% N_2) at operating gas pressures corresponding to tissue spheres 2.0 , 4.0 and 8.0 μm in diameter. The results of these measurements indicated satisfactory performance of counters to measure microdosimetric spectra extending down to event-sizes that cover the gamma component of a mixed field. The spectra and the related mean values $\bar{y}_F$ and $\bar{y}_D$ are compared with other similar work but with monoenergetic neutrons of different energy range, the agreement between them is good.

An assessment of the performance of different size TEPC has been done. An excellent agreement between their event size spectra was found and the proton edge appears at the same position on the lineal energy scale and differences in microdosimetric parameters $\bar{y}_F$ and $\bar{y}_D$ is not exceeding 3%, which is in the region of counting statistics.

In Am-Be neutron field, the efficiency of the TEPCs was measured to have an average value of 250 counts per μSv or equivalently about 4.17 counts per minutes per μSv/hr. This efficiency is reasonable for dose equivalent measurements but needs a long integration period. The measurements showed that the dose equivalent which depends on the measurement of energy deposition by the secondary charged particles was originated mainly from elastic collisions of the incident neutrons with hydrogen atoms. Moreover the number of events in the sensitive gas is dominated by proton recoils. A non-negligible fraction of the dose equivalent resulted from gamma interactions, alpha and recoil nuclei.

The energy deposition patterns in these micro-scale targets are strongly dependent on radiation quality, so differences of linear energy transfer (LET) of the components in a mixed radiation field are significant. Accordingly, in a radiation field with an unknown gamma ray energy spectrum, absorbed dose for neutrons can be obtained by the separation of neutron induced events from gamma events using their distribution in lineal energy. To separate neutron dose from gamma dose a simple lineal energy threshold technique has been used in addition to a more sophisticated methods using γ-fitting and the graphite-walled counter measurements. The results of this study will establish the degree of error introduced by using a lineal energy threshold, which is likely to be used in any hand-held neutron monitor based on TEPCs.

Keywords : Microdosimetry, TEPC, GPC, Mixed Field Dosimetry, Am-Be Neutron Source

TABLE OF CONTENTS

ACKNOWLEDGEMENTS

I wish to express my sincere gratitude and appreciation to my supervisor Dr. Anthony Waker for his guidance, supervision and encouragement during my research. His invaluable assistance, patience and support helped me a lot.

I would also like to thank the University of Ontario Institute of Technology (UOIT) for the given opportunity to complete my graduate study.

I extend my gratitude to the support of all the staff of the Faculty of Energy Systems and Nuclear Science and to thank all my colleagues and friends for their help during my study. Special thanks go to Mr. Fawaz Ali for his helpful comments.

I am grateful to the University Network of Excellence in Nuclear Engineering (UNENE) and the Natural Science and Engineering Council of Canada (NSERC) for their financial contribution to this research.

Finally, I am indebted to my family for their continued support and patience throughout my life and particularly during this chapter of our life.

LIST OF FIGURES

LIST OF TABLES

NOMENCLATURE

CF	Calibration Factor, keV/µm/Channel Number
D	Absorbed Dose, Gy
d_d	Diameter of the Counter, µm
d_t	Diameter of the Tissue, µm
d(y)	Dose Probability Density
d_n	Absorbed Dose from Neutron, Gy
d_γ	Absorbed Dose from Gamma, Gy
E_g	Energy Deposition in the Gas Material of the Counter, keV
E_t	Energy Deposited in the Tissue, keV
f(y)	Lineal Energy Frequency Distribution
H	Dose Equivalent, Sv
h	Pulse Height
h_c	Mean Pulse height, Channel
LET	Linear Energy Transfer, keV/ µm
M_d	Mass of the Gas in the Cavity, kg
$\overline{Q}$	Average Quality Factor,
P	Required Pressure, Torr
S	Surface Area of the Body, cm2
W_r	Radiation Weighting Factor
X_t	Path Length Across the Simulated Tissue, µm
X_g	Path Length Across the Gas Cavity, cm
y	Lineal Energy, keV/µm

ε	Imparted Energy, keV
$\bar{l}$	Mean Chord Length, μm
$\bar{Q}$	Mean Quality Factor
ρ_g	Density of Gas, kg/m^3
ρ_t	Density of Tissue, kg/m^3
$\bar{y}_F$	Frequency mean Lineal Energy, keV/µm
$\bar{y}_D$	Dose Mean Lineal Energy, keV/µm
$\bar{y}_\alpha$	Lineal Energy for α Source, keV/µm
σ	Statistical Uncertainty ,%

Acronyms

ADC	Analog to Digital Converter
DPP	*Digital Pulse Processor*
GPC	Graphite Proportional Counter
ICRP	International Commission on Radiological Protection
ICRU	International Commission on Radiological Units
MCA	Multi Channel Analyser
TEPC	Tissue Equivalent Proportional Counter
UOIT	University of Ontario Institute of Technology

Chapter One : INTRODUCTION

1.1 Introduction to Mixed Field Radiation and Dosimetry

Mixed fields are those composed by radiation of different types and/or energy, e.g. gamma photons and electrons, photons and neutrons or even neutrons with sufficiently different energy, share some of the characteristics of a mixed field. Mixed field are the common type of radiation fields, although in some practices, the doses caused by one of the field components are more significant, so that the contribution of the others can be neglected.

The radiation fields due to cosmic rays, natural radioactive isotopes, medical diagnostics, nuclear reactors and radioactive sources used in industry are mostly mixed fields due to the complexity of the charged particle energy spectrum which leads to the deposition of energy. Extensive studies on radiation applications, lead researchers to conclude that, neutron and photons are important contributors to dosimetry. As an example, the dose equivalent outside a thick shield of high-energy particle accelerators is mainly due to neutrons, with some contribution from photons and, to a minor extent, charged particles. At high-energy electron accelerators, the dominant secondary radiations are high energy neutrons and bremsstrahlung photons. Nuclear fusion experimental facilities produce high flux of fast neutrons and the resulting radiation fields at workplaces, out of the concrete shielding that encase the main fusion facilities, are dominated by thermal neutrons but fast neutrons and photons are also present[1]. At flight altitudes, similar radiation fields are encountered, and it is actually possible to partly 'simulate' the radiation field in the atmosphere with accelerator-produced radiation[2].

Radiation protection science, uses a system of units which is based upon the concept of absorbed dose and dose equivalent which has been found to work well for simple radiation fields, however, the monitoring of radiation which comes from complex radiation fields, appears to be a difficult task because of the necessity of properly identifying the contribution of each field component.

The International Commission on Radiological Protection (ICRP) in its report 60 (ICRP 60, 1990), immediately after proposing the Absorbed Dose (D) as the fundamental dosimetric quantity in radiological protection, introduces the radiation weighting factors (w_R) and defines the Equivalent Dose (H) as the product of both, D and w_R, and states: "When the radiation field is composed of types and energies with different values of w_R, the absorbed dose must be subdivided in blocks, each with its own value of w_R and summed to give the total equivalent dose"[3].

Therefore, for a suitable dosimeter with acceptable analysis capability for mixed fields and its components, the first requirement is the independent determination of the absorbed dose caused by each field component with different w_R.

Absorbed dose is, in fact, the most applicable dosimetric quantity which is defined as the quotient of the imparted energy to matter divided by the relevant mass. One way to determine absorbed dose is the application of cavity theory. The fundamental basis of all cavity theories is the determination of absorbed dose in a medium by measuring the absorbed dose inside a cavity gas which is introduced in the medium. Some generalized cavity theories have been developed for dealing with the situation in which the cavity size is not small in comparison with the secondary charged particles ranges which is, in general, a necessary condition for the application of cavity theory.

A direct method by which absorbed dose to a gas cavity can be determined is by using low pressure tissue equivalent proportional counter (TEPC) , which can be used for radiation monitoring in areas where a mixture of neutrons and photon radiations may be present. TEPCs are widely used as the main tool in experimental microdosimetry measurements, which means the measurement of the absorbed dose in an event by event manner inside a tissue equivalent unit-density simulated site diameter of the order of micrometers in diameter[4].

Generally, the measurement of dose rate on the microscopic scale or the study of energy deposition in cellular and subcellular targets, is termed Microdosimetry.

Furthermore by interpretation of the event-size spectrum recorded during the measurement, valuable information can be obtained enabling some analysis of the radiation field to be made. Applications of microdosimetric techniques allow the use of lineal energy event-size spectra (microdosimetric spectra) to determine the values of the dose contribution by different types of particles, i.e. by obtaining information about the components of an unknown radiation field, to understand the mechanisms of radiation interaction physics, and enabling the measurement of absorbed dose, dose equivalent and mean quality factor[5] as well as a physical means of quantifying radiation quality with regards to biological effects.

1.2 The Importance of Microdosimetry in Mixed Field

Most of the radiation which comes from natural and artificial sources produces a mixed radiation field. Even some single radiation type can give rise to mixed field because it generates other types of radiation through its interaction with matter, i.e.

thermal neutrons captured by hydrogen contaminate the neutron field with high energy gamma-rays.

In radiobiology, humans exposed to ionizing radiation, are known to undergo a wide variety of biological effects, including mutations, cell death, chromosome aberrations and carcinogenic transformations. Most effects of direct relevance to humans, whether from environmental, occupational, diagnostic, or therapeutic exposures are due to damage induced by energy deposited in the form of highly structured tracks of atomic ionization and excitation along the path of the primary and secondary charged particles in individual cells. The ionization pattern in the track has a direct impact on the cellular mechanisms and so there is a very great need to understand the structure of the radiation field and the way that the individual tracks and hence the energy deposition at the cellular and the subcellular level[6].

Recently, the development in the use of radiotherapy application, especially the use of advanced proton and neutron therapy facilities, has stimulated the need for further studies in mixed field dosimetry through the use of microdosimetric measurements to specify the beam quality in treatment fields.

Mixed fields of neutron and gamma radiations represent significant challenges to operational health physicists working in nuclear power plants or near particle accelerators. The range of neutron energies and field intensities encountered give rise to significant instrument design problems, which the application of microdosimetric methods can help.

1.3 General Principle and the Application of Microdosimetry

Experimental microdosimetry measures the absorbed dose in an event by event manner inside a tissue equivalent unit density simulated site diameter of the order of micrometers[4]. The instrument which is widely used for this purpose is the tissue equivalent proportional counter (TEPC). A detailed description of this type of device is given later in this work.

Low pressure TEPCs provide a more direct method by which the absorbed dose to a gas cavity can be determined by measuring the individual energy deposition events of secondaries produced by the interaction of neutrons and gammas. Furthermore by interpretation of the event-size spectrum recorded during the measurement, valuable information can be obtained enabling some analysis of the radiation field to be made.

Applications of microdosimetry techniques can be used to detect and determine the values of the dose contributions by different types of particles, i.e. obtaining information about the components of unknown radiation fields, in addition to understanding of the mechanisms of radiation effects.

1.4 Thesis Objectives

The main objective of this study was to determine the absorbed dose, quality factors, and dose equivalent under mixed neutron gamma field conditions for the UOIT Am-Be neutron source by using different sizes and types of proportional counters employing microdosimetric techniques. The microdosimetric spectra obtained were compared also to other published neutron energy spectra to have a clear picture of the

contribution of each type of radiation to the total absorbed dose and of their respective microdosimetric spectra.

Subsidiary to this principle objective, two minor objectives were also the subject of investigation. The first one was to verify the validity of the generalized cavity theory for high energy neutron spectrum of the Am-Be source by using a graphite proportional counter. And the second was to establish the degree of error introduced by using a lineal energy threshold to separate the neutron dose from gamma dose, by comparing with more sophisticated methods using a pure gamma source fitting and the graphite walled counter measurements.

1.5 Summary of the contents of this Work

The main purpose of this work was to promote understanding of the dosimetry of Am-Be neutron source by applying microdosimetric techniques. Thus chapter two deals with an introduction to microdosimetry as a multi-application technique in radiation dosimetry. Microdosimetric experimental procedures, quantities and parameters as well as the proportional counters used in microdosimetry are described. Tissue equivalent plastic and gases involved in the application of TEPCs and the method of simulating unit density microdosimetric tissue equivalent volumes and the factors involved are also explained and described. Finally representation of the distribution and applications of experimental microdosimetry are discussed.

In chapter three the UOIT neutron facility is described. Characteristics of the used TEPC and GPC including, operation, calibration and measuring electronics are explained. The method of spectra representation and dosimetry quantity calculations are described

and finally chapter three ends with a review of neutron gamma discrimination techniques and the method of uncertainty analysis.

In chapter four a series of microdosimetric measurements with simulated diameters, ranging from 2 μm to 8 μm have been carried out at the Am-Be neutron source and compared with other published spectra. Frequency distribution spectra in a graphite proportional counter were measured and the generalized cavity theory applied to analyse the similarities and the differences observed between Am-Be neutrons and low energy neutrons previously measured[7].

Chapter five presents the general conclusions of the work and also the necessary and important directions which could be pursued for this type of investigation in the future.

1.6 A General Literature Review of Previous Experimental Microdosimetry

The technical suitability of microdosimetric instruments for measuring absorbed dose, average quality factor and dose equivalent for radiation protection purposes has been discussed thoroughly and has played an important role in the relevant literature for many years. In 1955, Rossi, in an attempt to experimentally measure LET introduced his LET spectrometer, which is nowadays called the "Rossi Counter", which was a low pressure proportional counter LPPC consisting of a spherical chamber of 2 cm diameter filled with a low pressure gas to simulate a 1 μm tissue site. Rossi discovered through using his counter that the measurement data represented the actual energy distributions which would determine the effect of the radiation on a cell. This is what was called at that time 'stochastic dosimetry' and later as micrdosimetry[8].

To simulate and measure the probability of local energy densities and the energies imparted to submicroscopic regions in the cell, Rossi designed refined instrumentation, such as the tissue equivalent spherical proportional counter. The term experimental Microdosimetry is usually reserved to describe work based on the use of low pressure tissue equivalent proportional counters[9]. Later, TEPCs became a versatile tool in exploring the field of radiation science and to measure the dose parameters on the microscopic scale.

Early microdosimetric measurements of event distributions for a wide range of photons energies (below 10 MeV) and a different site sizes, carried out by Rossi, Biavati and Gross and others indicated that for different gamma sources of low LET radiation, there are a large differences in event size for different energies[10] the event size spectrum arises from the deposition of energy from the secondary electrons produced by the primary interaction of photons with the counter wall and gas filling.

In 1960, Columbia University and Brookhaven National Laboratory began experimental investigations which built the groundwork for the radiobiology of neutrons and through neutrons for the radiobiology of densely ionizing radiations. For the first time it was realised then that neutrons can, at small doses, be vastly more effective than photons. The reason of the complexity of neutrons upon photons are the generating of more than one type of charged particle, each has its own energy spectrum and interaction properties[9]. For a better understanding of the interaction of neutrons with tissue, extensive experimental and theoretical studies on the distribution patterns of energy deposition in small tissue spheres (d = 0.1 μm to 10 μm) irradiated by neutron beams have been established[11,12,13].

Microdosimetric measurements of neutron radiation are important in radiation protection studies, helping to evaluate the radiation quality factor for better estimation of the dose equivalent[14]. Booz has described the advantage of microdosimetric methods in radiation protection, showing that there is good correlation between Q and $\bar{y}_D$, the dose mean of microdosimetric spectra, as a function of LET. Microdosimetric proportional counters can be used to evaluate the neutron and gamma dose fractions of unknown radiation field without recurrence to other instruments and methods[15].

TEPC response has been improved by many researchers through the modification of the detector themselves by increasing the wall thickness, reducing the filling pressure, altering the gas composition, or some combination thereof[16,17,18]. The main problem that faces the improving process was that improving the response in one energy range tended to degrade the response in other regions.

Decades of experience in doing experimental microdosimetry under a variety of conditions and with an extensive assortment of counters, helps to identify most of the sources of systematic error[19]. Major sources of error are extrapolation errors, statistics, energy calibration, pulse rate (pile-up effects), zero setting (ADC), gas gain (drift), pressure measurement, and the determination of mean chord length. Uncertainty in microdosimetric parameters estimated to reach 10%[20]. The situation is more exacerbated for high energy neutrons, with focus on calibration, wall effects, W values and stopping power[21,22]. Electronic sources of error can be minimized or effectively eliminated by using new electronics for measurements. Digital pulse processing seems to be very promising with its highest throughput and lowest dead time.

To separate the absorbed dose distributions in lineal energy for neutron from those for gamma rays in mixed field, different techniques have been used. Some techniques required the knowledge of energy spectra and dose distribution of gamma rays, and others overcome this problem by using a graphite proportional counter along with the tissue equivalent proportional counters.[23,24,25].

Chapter Two : Microdosimetry Background

2.1 Historical Background and General Description of Microdosimetry

Ionizing radiation is a source of a variety of biological effects, including mutations, chromosome aberrations, cell death and carcinogenic transformations. The detailed understanding of the mechanisms by which these effects are induced are related to the microscopic patterns of interaction and energy deposition.

Microdosimetry which was earlier called "stochastic dosimetry" as a branch of radiation science is defined by Rossi and Zaider[26] as " the systematic study and quantification of the spatial and temporal distribution of absorbed energy in irradiated matter" . In general, microdosimetry is the measurement of absorbed dose on a microscopic scale. In other words, microdosimetry is related to the energy which has been stochastically deposited in a medium of microscopic dimension, the distribution of this imparted energy depends on the radiation type or quality.

Attempts have been made to build a direct link between microdosimetric quantities which are used to characterize radiation fields to the observed effects of radiation on biological cells and to use them as a predictive tool of, Relative Biological Effectiveness (RBE). The Theory of dual radiation action (TDRA) proposed by Kellerer and Rossi in 1972 is one such[27]. It has been considered by many investigators that radio-sensitive sites in biological specimens are of the order of 1 μm in dimension. Hence linear dimensions of about 0.1 μm to 10 μm have been simulated and applied for much experimental and theoretical microdosimetric work.

2.1.1 Experimental Microdosimetry

The study and interpretation of single-event energy deposition spectra measured using low pressure proportional counters to simulate microscopic site of tissue is called "Experimental Microdosimetry". The energy that a charged particle looses when it passes through a TEPC gas cavity can be related to the energy which would be lost along a microscopic path length within a tissue medium of unit density. The distribution of the deposited energy will be related to LET (Linear Energy Transfer) of the radiation but taking into consideration all the related stochastic effects (i.e. energy loss straggling, energy transport due to delta rays, variation of LET along the track and finite path length of particles). The density difference between the gas and the tissue enables the simulation by the counter of a microscopic tissue volume. A single interaction event in the cavity gas will produce a voltage pulse of measured amplitude proportional to the amount of imparted energy. The spectrum of pulse heights reflects the stochastic nature of the deposited energy. The frequency of events measured for different event-sizes allows the absorbed dose to be determined. The dose equivalent can be evaluated by the same method using an appropriate quality factor approximation. A set of measurable microdosimetric quantities and some parameters which represent the basis of the experimental microdosimetric will be explained in the next section.

2.1.2 Microdosimetric Quantities and Parameters

The fundamental quantity applied in microdosimetry studies is the energy deposited $\boldsymbol{\varepsilon}_i$ in joule (or eV). The energy deposited (imparted energy) $\boldsymbol{\varepsilon}_i$ is the energy

deposited in a single interaction, so the energy deposited by ionizing radiation to matter will be :

$$\varepsilon_i = T_{in} - T_{out} + \sum Q \qquad (2.1)$$

Where T_{in} is the sum of all energies relating to all ionizing particles which enter the volume (excluding rest mass) , T_{out} is the sum of all energies relating to all ionizing particles leaving the volume, and $\sum Q$ is the sum of all variations of the rest mass energy of all atoms and all elementary particles which are involved in interaction.

Energy imparted in joule (or eV), $\boldsymbol{\varepsilon}$ is the summation of all energy deposition $\boldsymbol{\varepsilon}_i$ by individual ionizing radiation events in a given volume :

$$\varepsilon = \sum \varepsilon i \qquad (2.2)$$

Energy deposition has a random nature which indicates the stochastic nature of imparted energy.

The specific energy Z is the quotient of the energy imparted by ionization radiation to the mass m :

$$Z = \varepsilon / m \qquad (2.3)$$

The unit of specific energy Z is joule per Kilogram (J/kg), which is usually expressed in Gray (Gy).

The stochastic quantity lineal energy '**y**' is the quotient of the imparted energy $\boldsymbol{\varepsilon}$ by $\bar{l}$, the mean chord length in the volume of interest :

$$y = \varepsilon / \bar{l} \qquad (2.4)$$

Lineal energy is presented in units of keV/μm . $\bar{l}$ is the mean chord length for the site , which is the mean length of randomly oriented chords in that volume. For a spherical counter of diameter d, mean chord length $\bar{l}$ = 2/3 * d. This expression are derived from the Cauchy Theorem[28]for convex bodies of $\bar{l}$ = 4.V / S, where V is sphere volume = 1/6 . π . d^3 and S is sphere surface area= π.d^2 .

In microscopic dimensions, where the fluctuation in energy deposition becomes of increasing importance, specific energy is the appropriate description of energy deposition instead of average absorbed dose.

When particles interact with a given volume, they can release, with different probabilities different quantities of energy, which generate a broad spectrum of lineal energy. The distribution of the number of events with event size between y and y+dy shall be denoted the frequency distribution of y as f(y). The mean value of f(y) is defined as the frequency-mean lineal energy $\bar{y}_F$ which can be expressed by the following equation:

$$\bar{y}_F = \int_0^\infty y.f(y)dy \,/\, \int_0^\infty f(y)dy \qquad (2.5)$$

The dose distribution d(y) is defined as the normalised distribution of the product y.f(y) and represent the relative contribution of the event y to the dose. The mean value of y.f(y) is defined as the dose-mean lineal energy $\bar{y}_D$, expressed as :

$$\bar{y}_D = \int_0^\infty y\text{^}2.f(y)dy \,/\, \int_0^\infty yf(y)dy \qquad (2.6)$$

Since by definition for normalized distribution $\int_0^\infty f(y)dy = 1$

$$\bar{y}_D = (1/\bar{y}_F).\ \int_0^\infty y\text{^}2.f(y)dy \qquad (2.7)$$

2.2 An Introduction to Microdosimetric Experimental Methods

Although, detection of radiation and the measurement of absorbed dose can be done through a variety of methods. It is preferred mostly in radiation dosimetry and microdosimetry to use the gas-filled detectors, in general, and low pressure tissue equivalent proportional counters, in particular. The reason for this is obvious, TEPCs were constructed to mimic the elemental composition of biological tissue of microscopic site size with the ability to measure the absorbed dose as a function of a stochastic quantity related to LET (Linear Energy Transfer) This is achieved by choosing the wall material and sensitive volume gas composition from materials similar in composition to tissue, controlling the pressure to give a suitable site size.

2.2.1 Mixed Field Sources : Neutron and Gamma Sources

In mixed neutron-gamma field dosimetry measurements, each part of the radiation makes a specific contribution to the dose equivalent. Some important factors about the nature of the mixed field need to be taken into consideration, these are:

First: to measure the gamma part most of the photons must have a sufficient energy to penetrate the counter wall, which is the case in most of the common accompanying photon fields; neutrons by their nature are always a penetrating radiation.

Second: the very different quality factors defined for neutrons depending on their energy is one of the distinguishing features of neutron fields. With gamma radiation present in the external field; a component with unity quality factor should be added. For this reason, dose equivalent measurement in neutron-gamma field is a complicated process, as the sole measurement of the absorbed dose is not sufficient.

Third: To build a suitable neutron dosemeter, tissue equivalence in principle should be in the exact atomic composition of the material and not only equivalence in the effective atomic number, as in the case of photons. This is a rather restrictive requirement, nearly impossible to fulfil in practice.

Microdosimetric techniques (TEPCs) are the only methods which can be applied to an acceptable extent and can identify the contribution of low and high LET components with a single detector.

To understand the way TEPCs work, we need first to know the modes of gamma and neutron interaction with matter. As an indirectly ionising radiation, gamma rays make a primary interaction with matter, depending on the energy of photons, through the processes of the photoelectric effect, Compton scattering and pair production, producing energetic secondary electrons (charged particles). It is the interaction of the secondary electrons themselves which lead to the deposition of energy in matter. Gamma ray dosimetry is mostly related to the complexity of the electron energy spectrum which leads to the deposition of energy.

There are many different ways of interaction of neutrons with tissue and tissue equivalent materials, depending mainly on neutron energy. The secondary radiations

resulting from neutron interactions are almost always heavy charged particles. These particles may be produced either as a result of neutron induced nuclear reactions or they may be the nuclei of the absorbing material itself, which have gained energy as a result of neutron collisions. The relative contribution to the dose equivalent from neutrons interacting with tissue (which consists mainly of hydrogen H, , carbon C, nitrogen N and Oxygen O) is a consequence of the following interaction mechanisms according to neutron energy:

1- Fast neutrons interacting with carbon and oxygen via non elastic scattering and result in the release of charged α particle. At different threshold energies, Inelastic scattering (n,n') which has a very low cross section, may emit gamma photons and heavy recoil nuclei. As examples the threshold for oxygen is 6 MeV and cannot occur with hydrogen. The relative contribution of the C, N and O recoils to the dose equivalent is greater than for the absorbed dose because of their higher average value of LET (i.e., larger quality factors) .

2- Intermediate energy neutrons above 100 eV[29], interact primarily with hydrogen nuclei via elastic scattering producing recoil protons. Hydrogen has a large macroscopic cross section for elastic scattering and it is the most abundant atom in tissue which have the same mass as neutrons.

3- Absorption is the dominant interaction mechanism for thermal neutrons in tissue and is followed by activation. Two capture reactions are important for neutrons in thermal region, those are $^{1}H(n,\gamma)^{2}H$ and the $^{14}N(n,p)^{14}C$ reactions which produce gamma of 2.2 MeV and proton of 0.58 MeV energy. The second reaction yields greater energy for local deposition than the incident neutron.

2.2.2 Proportional Counters in Microdosimetry

The fundamental principle behind a proportional counter, which is similar to all other radiation detection instruments, is to detect and measure the changes produced by the interaction of radiation with the detector medium. The detector medium in proportional counters is a gas. The radiation interaction with the gas will generate a number of ion pairs related to the size of the energy deposition event.

The free electrons resulting from an ionizing event can gain sufficient kinetic energy due to an increasing electric field to ionize other gas molecules in their paths; this process is called the Gas gain or 'multiplication'. Thus because of the gas multiplication process a single electron can produce an electron avalanche. The gas gain 'G' for each of the primary ionizations can be defined as the average number of electrons collected at the anode. Two important factors which determine the gas gain are the electric field strength and gas pressure of the sensitive volume of the counter.

Gas multiplication requires large values of the electric field. In cylindrical geometry, the electric field at a radius r is given by[30] :

$$E(r) = (1/ r) . (V_{ab} / \ln (b/a)) \qquad (2.8)$$

Where V_{ab} is voltage applied between anode and cathode, a is anode wire radius and b is cathode inner radius.

It can be seen from equation (2.8) that if 'r' decreases the value of the electric field strength is increasing rapidly and the process of gas multiplication begins in a region which is very close to the anode. Gas amplification does not therefore depend on the

position of formation of the primary ions, and there will be proportionality between the resulting pulse and the number of primary ions.

As the gas pressure inside the counter is lowered, the more the multiplication zone extends toward the cathode[31]. This factor will limit the site size which can be simulated.

Let dr is an elemental distance in the direction of the electric field; the following general equation represents the gas gain for the multiplication process:

$$\text{Ln G} = \int_a^b \alpha \, . \, \text{dr} \qquad (2.9)$$

where 'α' is Townsend's first ionisation coefficient and represents the number of ion pairs produced by one primary electron per unit path length[30]. It increases with increasing the electric field and decreases with increasing the pressure since the smaller the mean free path, the less time a particle has to reach sufficient ionization energy between collisions. So α is related to the reduced field strength 'E/P', where 'P' is the gas pressure.

The following equations have been proposed to describe the functional relationship between α and the reduced field strength[31]

$$\alpha/P = A \, . \, \exp(-B.P/E) \qquad (2.10)$$

Where A and B are constants for any given gas. Substituting equation (2.9) in equation (2.8) yields:

$$\text{Ln (G)} = \int_a^b P.A.\exp[(- B.P.V_{ab} / \text{Ln (b/a)}).1/r.dr] \qquad (2.11)$$

In integration of equation (2.11) yields the expression for the gas amplification in the electric field of a cylindrical counter as:

$$\text{Ln (G)} = \frac{A}{B} \cdot \frac{V}{\text{Ln}\left(\frac{b}{a}\right)} \cdot [\exp(- \frac{a.B.P.\text{Ln}\left(\frac{b}{a}\right)}{V}) - \exp(- \frac{b.B.P.\text{Ln}\left(\frac{b}{a}\right)}{V})] \qquad (2.12)$$

In this equation the constant 'A' is referred to the reciprocal of mean free path at unit pressure and the constant 'B' refers to the ratio between the effective ionization potential and the mean free path. As an approximation the exponential parts can be eliminated resulting in a linear relationship between Ln G and V. Figure 2.1 shows the gain-voltage characteristics for the GPC used in this study operated at a gas pressure of 55.6 torr corresponding to a site size of 2μm. As the constant 'A' and 'B' are known to vary with reduced field strength, the relative gain of the counter has been determined experimentally and plotted against the applied anode voltage. The relative gas gain is given by :

$$G^* = [Ch.(N_i)/Ch.(N_0)] \cdot (A_0/A_i) \qquad (2.13)$$

Where A_0 and N_0 indicate the reference amplification and channel N_0 for the peak produced by the internal calibration source at a given anode voltage, and A_i and N_i indicate the amplification and the channel N_i for the alpha peak at higher applied anode potentials.

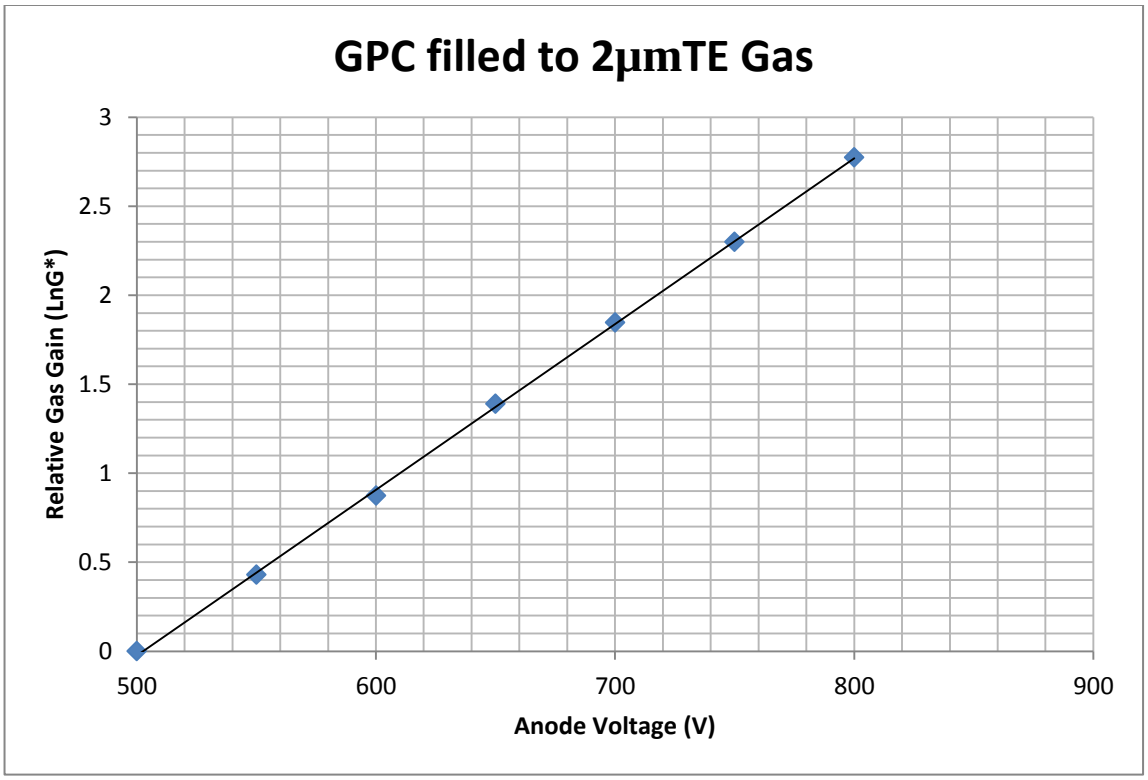

Figure 2.1 Gas gain-voltage characteristic for the GPC filled to 55.6 Torr TE gas to simulate a diameter of 2µm.

2.2.3 Tissue Equivalent Plastics and Gases

The low pressure TEPC is normally constructed of tissue equivalent plastic, namely Shonka A-150 and filled with tissue equivalent gas[32]. The shonka A-150 plastic contains the same elements closely related to what has been suggested by ICRU as standard muscle tissue[33]. There is no ideal tissue equivalent material which can be applied for all radiation energies used in all microdosimetric measurements. Essentially, a tissue equivalent material for detector construction should have the property of electrical conductivity, and in order to make the shonka A-150 conductive and more suitable for gas detector construction, some oxygen has been replaced by carbon. By referring to table

2.1 , it can be considered that the A-150 has a composition almost the same as muscle tissue. However, as it was mentioned there is a change of carbon for oxygen.

Good counting gases need to be as electropositive as possible, so that liberated electrons can remain free to form the electrical avalanche; so basically, the gas composition needs to be free of electronegative gases such as water vapour and oxygen. Srdoc (1970)[34] formulated a muscle equivalent gas based on propane (table 2.1), which shows the same multiplication factor with a lower voltage than when using the earlier muscle equivalent gas based on methane which was formulated by Rossi and Failla in 1956[35] .

No.	Name	H	C	N	O	F	others
1	ICRU tissue, muscle	10.2	12.3	3.5	72.9	-	1
2	Muscle-equivalent plastic A-150	10.1	77.6	3.5	5.2	1.7	-
3	Muscle-equivalent gas, propane based	10.3	56.9	3.5	29.3	-	-

Table 2.1 Elemental composition of muscle equivalent compounds and mixtures in percentage by weight.

2.2.4 Classification of Particle Tracks:

According to Bragg-Gray cavity theory, the measurement of the ionization in a gas cavity yields the absorbed dose in the wall material surrounding the cavity. TEPC forms a homogenous Bragg-Gray cavity device and it offers tissue equivalency. The wall thickness of the TEPC is chosen so that for the required indirectly ionizing radiation, charged particles equilibrium (CPE) is obtained. The wall thickness must be as least as thick as the maximum range of the secondary charged particles but not too thick to prevent reduction of the fluence as much as possible. If any charged particles of a given

type and energy entering the sensitive volume as a replace for identical particle of the same energy leaving it, charged particles equilibrium (CPE) is obtained. As an example, for 4.5 MeV neutrons, with protons as secondary charged particles, this means a minimum thickness of about 0.305 mm (the maximum range of 4.5 Mev protons) tissue equivalent plastic[36].

For the reasons of this study, to understand the energy imparted in the sensitive gas by a specified type of secondary charged particles, it is useful to distinguish between four classes of particles tracks depending on the location of their production with respect to the sensitive volume[37] (see Figure 2.2)

1- Insiders: particles originating and lose their entire energy in the sensitive volume.

2- Starters: particles originating and lose part of their entire energy in the sensitive volume.

3- Stoppers: Particles originating outside the sensitive volume and stop within the sensitive volume. depositing part of their entire energy in it.

4- Crossers: particles originating outside the sensitive volume and cross the sensitive volume, depositing part of their entire energy in it.

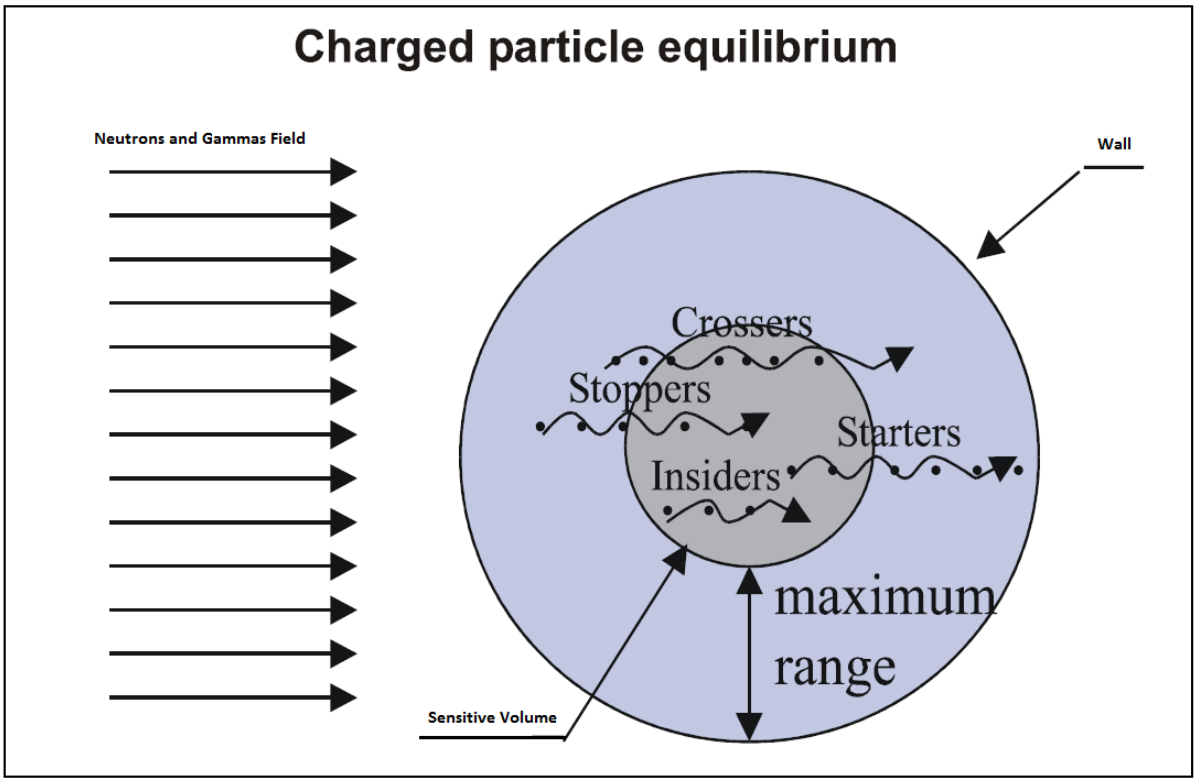

Figure 2.2 Classification of charged particle tracks with regard to their production with respect to the sensitive volume and counter wall

2.2.5 Simulation of Unit Density Microdosimetric Tissue Equivalent Volumes

The following principle is employed in order to simulate a unit density microscopic volume with a low pressure tissue equivalent gas:

The energy deposition in the tissue (E_t) should be equal to the energy deposition in the gas material of the detector (E_g) for the simulation to hold, thus:

$$E_g = E_t \qquad (2.14)$$

The energy deposited in a site, by a charged particle, is the product of the mass stopping power, the density of the medium and the path length of the ionizing radiation across the volume, That means[9] :

$$E_g = (dE/\rho dX)_g.\rho_g.\Delta X_g = E_t = (dE/\rho dX)_t.\rho_t.\Delta X_t \qquad (2.15)$$

Where E is the local energy deposition;

dE/ρdX is the mass stopping power of the target material;

ρ is the density of the target medium;

ΔX is the path-length across the target volume.

And the subscripts 'g' and 't' refer to the gas and tissue volume respectively. See Figure 2.3 .

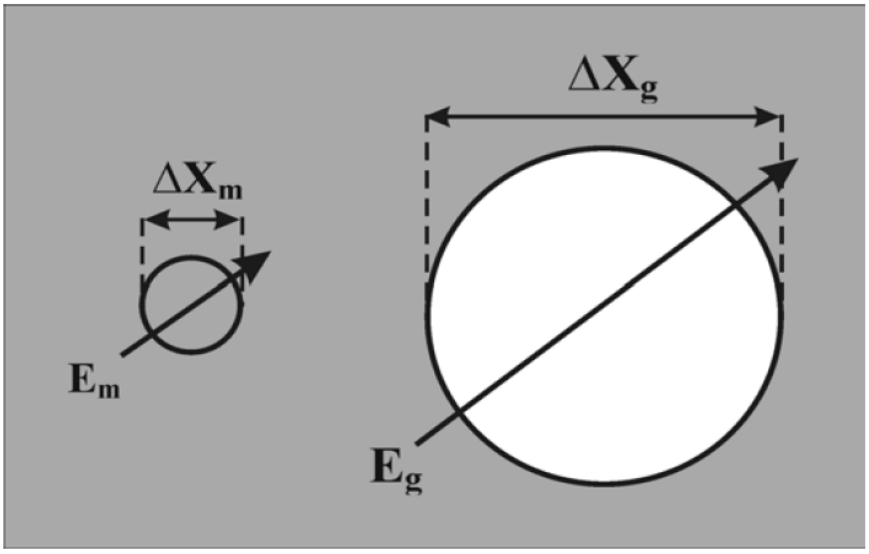

Figure 2.3 Microscopic tissue site size simulation using tissue equivalent gas cavity.

By definition tissue equivalence means have the same atomic composition, the mass stopping power of tissue and tissue equivalent gas are same.

$$\rho_g \,.\, \Delta X_g = \rho_t \,.\, \Delta X_t \qquad (2.16)$$

The density of the tissue, the size of the tissue volume, and the size of the detector volume are known. The gas density which controls the site size simulation, can be obtained from:

$$\rho_g = \rho_t \,.\, \Delta X_t / \Delta X_g \qquad (2.17)$$

These equations are used to calculate the density of the gas filling for any counter diameter to simulate any microscopic site size.

By using the gas density values in ideal gas equation :

$$P.V = n.R.T \qquad (2.18)$$

Where n is number of moles and equal the mass divided by the molecular weight.

The gas pressure required to simulate different site sizes can be written as:

$$P = (\rho/M).\, R.T \qquad (2.19)$$

To get the pressure P in Torr required to simulate different size sites using corresponding gas density values ρ in g/cm^3:

M=43.136 g/mole, molecular weight of propane based tissue equivalent gas

R=62.365X10^3 cm^3-torr/mole-^{0}K

T= 293 ^{0}K , Room temperature.

2.3 Representation of Microdosimetric Distributions

To explain the way to represent the measured microdosimetric distributions, we need first to have some essential understanding concerning the nature of events. The range of events sizes and hence pulse heights to be expected would cover several orders of magnitude from fractions of keV to thousands of keV. As an example, from mixed field radiation, the passage of a recoil

proton across the counter in a mixed neutron gamma radiation field is an expected type of event that might be depositing energy, at a rate of around 27 keV/μm, and will result in an event size of 36 keV for a 2 μm site size with mean chord length 1.33 μm. Gamma photons of 2.2 MeV which emits as a result of thermal neutron capture in hydrogen, will interact through Compton scattering producing fast electron which will deposit some 0.3 keV of energy. Fast neutron interaction with carbon will produce recoil carbon ion which can deposit some hundreds of keV of energy.

The problem of dealing with a large range of pulse sizes can be managed by redistributing the measured data into a scale constructed of equal logarithmic intervals of lineal energy[38]. The procedure of doing this and the way to analyse the results will be discussed in detail with some examples in chapter three.

Chapter Three : Experimental Methodology

3.1 Description of UOIT Neutron Facility

The UOIT neutron facility consists of three individual Am-Be sources of 1480 MBq (40 mCi) of ^{241}Am each. The Am-Be neutron source emits neutrons by using the 5.486 MeV alpha particles emitted by ^{241}Am via the reaction $^{9}Be(\alpha, n)^{12}C$. The ^{241}Am has a half-life of 432.2 years, so no decay correction is needed for the measurement period. The ISO reference neutron spectrum for Am-Be is showing in Figure 3.1[39]. An Am-Be source emits approximately $2.7X10^{6}$ neutrons per second per curie of ^{214}Am, which means that a neutron yield of approximately 70 ± 3 neutrons for 10^{6} alpha's can be achieved with ^{241}Am as an α-source. The UOIT neutron facility emits neutrons at the rate of $2.664X10^{5}$ neutrons per second having an average energy of 4.46 MeV with 14% of emitted neutrons having energy less than 1.5 MeV[40].

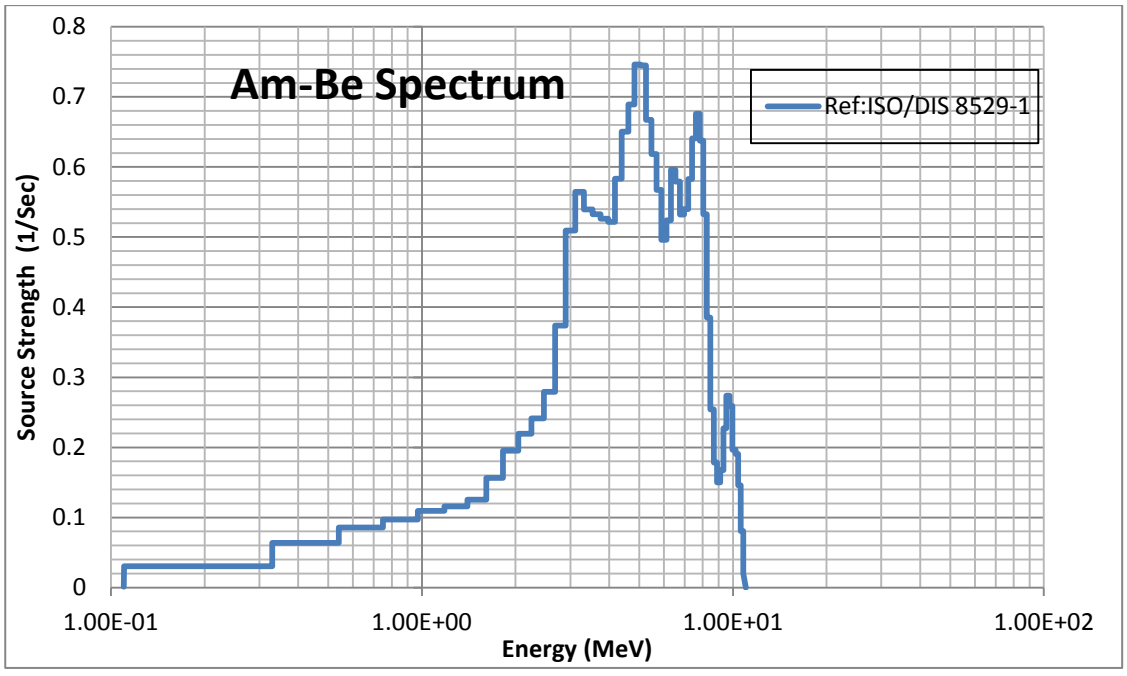

Figure 3.1 The ISO neutron spectrum of Am-Be

As neutrons are emitted anisotropically from the three Am-Be sources and neutrons will be scattered from the room walls, floor and ceiling, the neutron flux at 1 m distance from the source will only be approximated by equation 3.1 and figure 3.2 below:

Φ (neutron/cm^2.s) = Number of neutrons per sec / Area in cm^2

$$\Phi = \frac{A \,.\, N}{4 \,.\pi\, .r\text{^}2} \qquad (3.1)$$

Where A is the activity of Am-Be neutron source in α particles per second, and N is the number of neutron produced per 10^6 alpha particles emitted in the source.

A = 3*40 mCi = (3*40 * 10^{-3} Ci)* (3.7*10^{10} α particles / sec./Ci)

A = 4.44X10^9 α particles / sec.

Φ = (4.44X10^9 * (70 neutron/10^6 α particles)) / $4 \,.\pi\, .r\text{^}2$

Φ = 3.11X10^5 / $4 \,.\pi\, .r\text{^}2$ neutron/cm^2.s

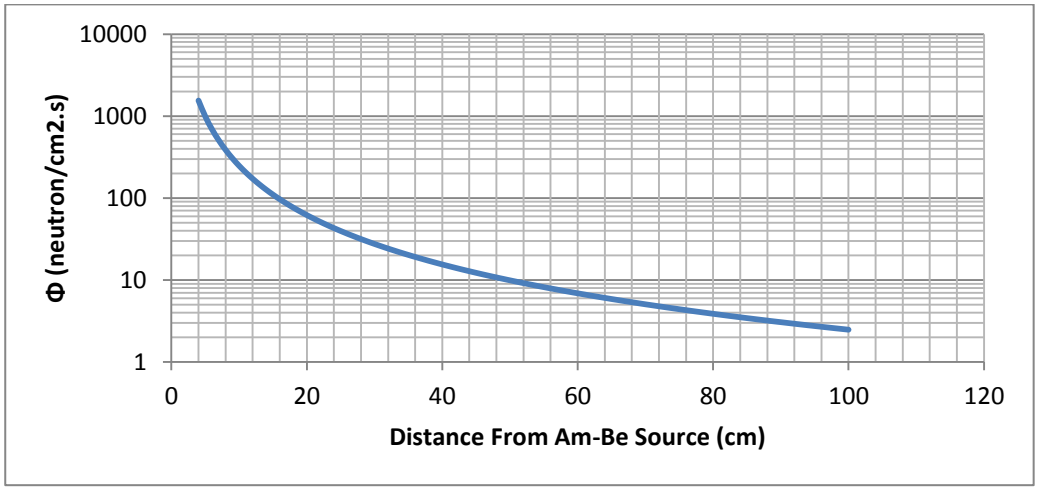

Figure 3.2 Calculated Am-Be neutron flux at varying distances from the source

Each neutron source is housed inside a vertical aluminum cylindrical tube. The whole facility contains nine vertical tubes arranged in a square lattice as (3X3 tubes). The sources are immersed in a water tank for shielding when they are not in use. The tank can be refilled without changing the shielding integrity using an in/out water circulation system. In order to sufficiently decrease the dose to acceptable levels, the water tank is located in the centre of a rectangular grid cage which provides adequate distance between the operator and source location. This facility is located in the basement of UOIT's engineering building, and was utilized to carry out all the experimental work. The location of the facility in the basement serves as an ideal location for research purpose because it is below ground and the concrete walls plus the earth surrounding the facility will provide more than sufficient shielding for neutron and γ-ray radiation.

A mechanical pulley system allows the three neutron sources to be raised in their respective aluminum tubes above the water level when measurements are taken or dropped within the water shielding when work is finished or in an emergency.

In order to carryout measurements, the counter was placed on a manually operated conveyor stand. The conveyor was operated from outside the cage and serves to bring the counters to the desired distance facing the neutron source.

The arrangement of the measurement setup with TEPC and GPC inside the neutron facility is shown in Figure 3.3.

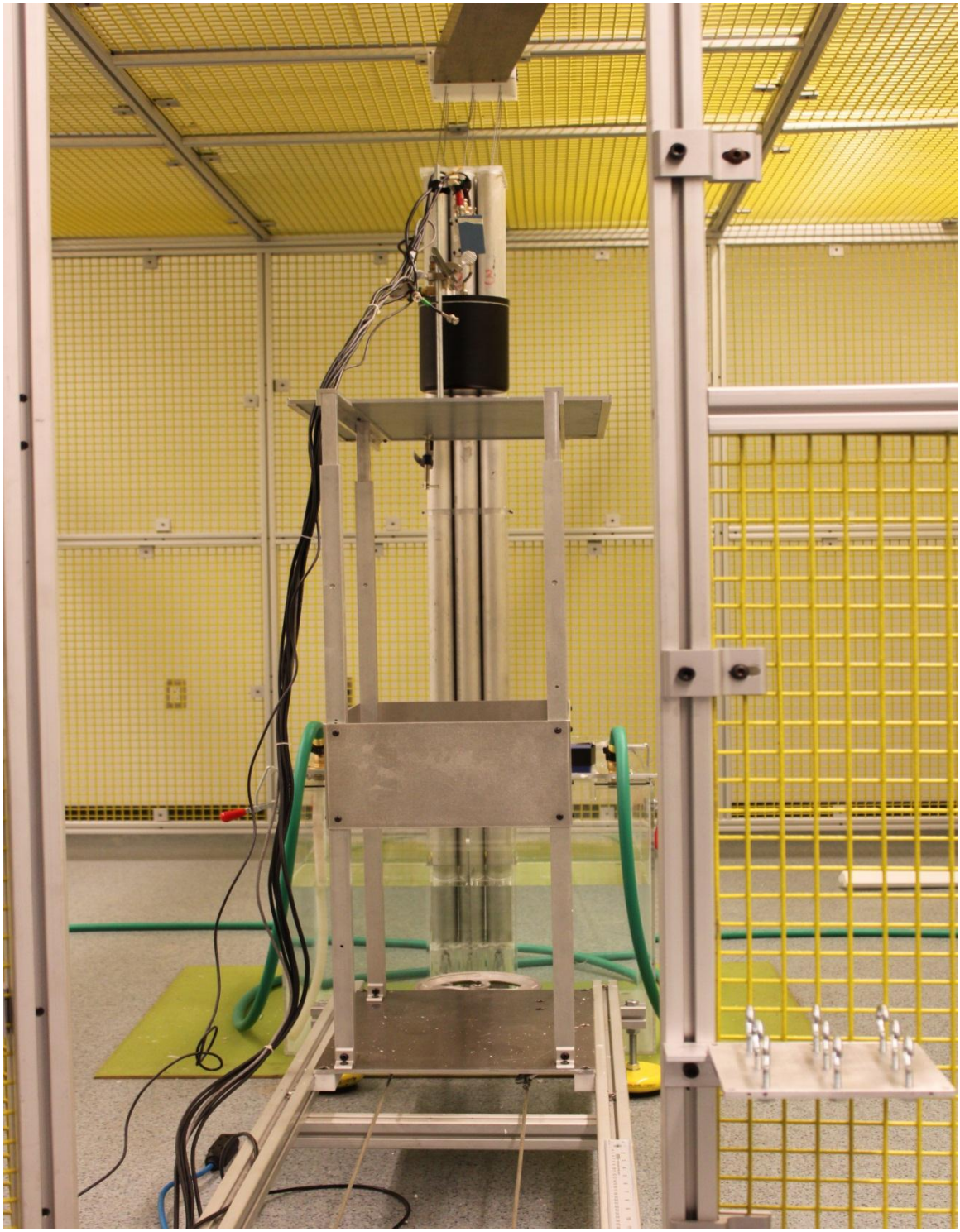

Figure 3.3 Arrangement for measurements with low pressure proportional counters at the UOIT neutron facility.

3.2 The Proportional Counters used in the course of the Current Study

3.2.1 The Counters:

A variety of procedures are used for the detection of radiation or to measure absorbed dose, but at the micron level which is the scale of measurements in experimental microdosimetry the primary and best available tool is the low pressure proportional counters. Three tissue equivalent proportional counters (TEPC), 12.7 cm diameter for two of them and 5.1 cm for the third were used in this study. A graphite walled proportional counter (GPC) of 1.5 cm diameter which was sensitive only to gamma and used to measure the gamma fraction in neutron gamma discrimination and to study cavity theory.

TEPCs were filled with TE gas to simulate three site size diameters of 2 µm, 4 µm and 8 µm while the GPC was filled to simulate a 2 µm site. Site size can be changed by changing gas pressure as shown in table 3.1 with some other important operational characteristics of the counters. The general characteristics of the TEPCs and GPC are shown in table 3.2. Three measurements for each site size were carried out.

D_t (μm)	$\bar{l}$ (μm)	ρ_g (Kg/m^3)			Pressure (Torr)		
		2"TEPC	5"TEPC	GPC	2" TEPC	5" TEPC	GPC
2	1.33	0.0392	0.0155	0.133	16.4	6.5	55.6
4	2.67	0.0784	0.031	0.267	32.8	13.0	111.0
8	5.33	0.157	0.062	0.533	65.6	26.0	222.0

Table 3.1 Gas pressure and density of the counting gas as a function of simulated size diameter.

Counter Characteristics	2 Inch TEPC	5 Inch TEPC	GPC
Geometrical Shape	Spherical	Spherical	Cylindrical
Overall Dimension (cm)	D = 5.1 cm	D = 12.7 cm	D = 1.5 cm
Volume (cm^3)	68.6	1072.5	1.77
Surface Area (cm^2)	81.1	506.7	7.068
Mass of Gas (mg) for 2μm site size	2.7	16.8	0.2355

Table 3.2 Comparison of general characteristics of standard TEPC and GPC employed in this study.

3.2.1.1 Tissue Equivalent Proportional Counters

A TEPC is a spherical cavity in tissue equivalent plastic (Shonka Type A-150) of a specified thickness, which is sufficient for proton equilibrium at least to 20 MeV. An aluminum can surrounds the TE plastic that provides electrostatic shielding and serves as a vacuum tight container. The collecting wire is positioned on a diameter of the sphere. A finely collimated internal ^{244}Cm alpha source introduces α particles of 5.8 MeV mean particle energy into the sensitive volume to calibrate the counter in terms of lineal energy[41].

Three proportional counters have been used in this investigation, produced and obtained from Far West Technology, California. Two were 5" (12.7 cm) in diameter and one was 2" (5.1 cm) in diameter. Their cross sectional view is shown in Figure 3.4.

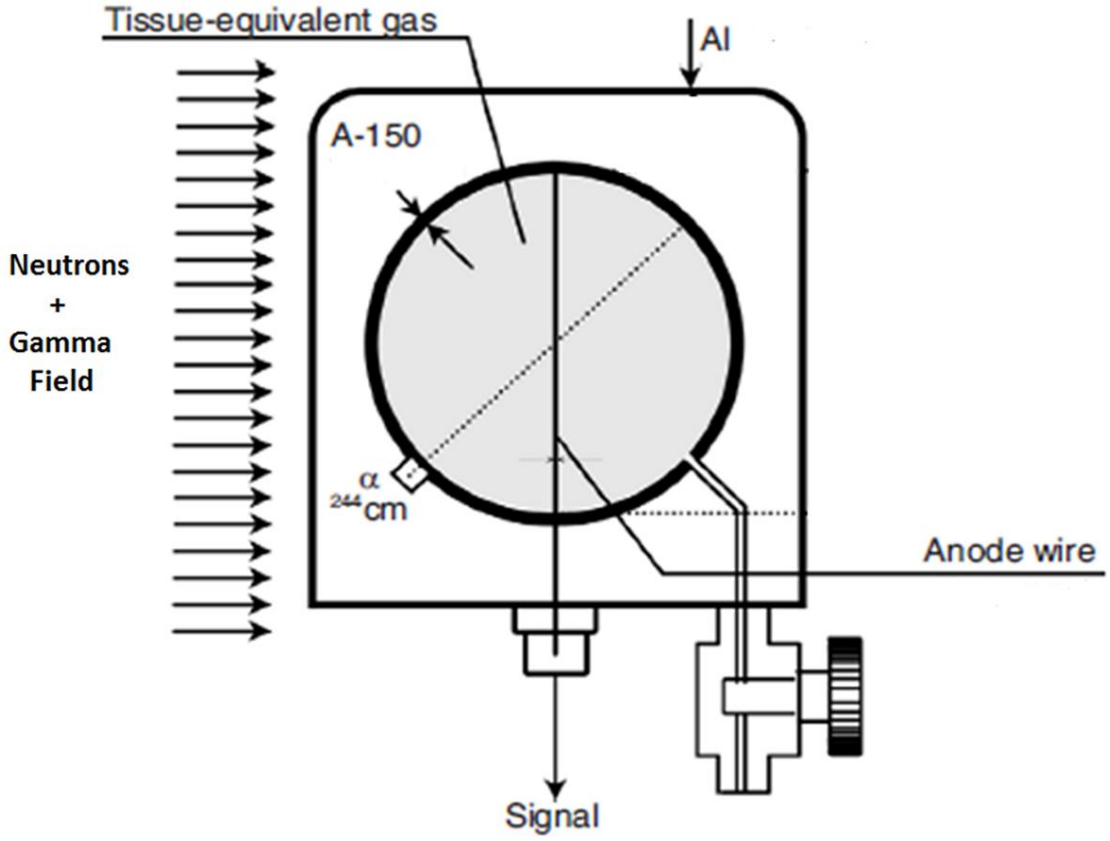

Figure 3.4 Cross sectional of TEPC

3.2.1.2 Graphite Proportional Counter

Figure 3.5 shows a line drawing of the graphite proportional counter GPC used in this study[42]. This counter with a sensitive volume defined by the wall and the field tube is a right-cylinder of 1.5 cm in diameter. The cathode cylinder and two field tubes, both machined from graphite. A gold plated tungsten wire of 50 μm in diameter is used as the anode for the counter. A finely collimated internal ^{241}Am alpha source introduces

monoenergetic α particles into the sensitive volume to calibrate the counter in terms of lineal energy. The calibration done through two holes machined in the side of the cathode, one in the center of the sensitive volume and the other one level with the end of one of the field tubes. When the α source is aligned to any of these holes, a beam of alpha particles deposits the energy in the sensitive volume of the counter. The alpha source can either be positioned over the collimating holes or be blocked by the wall of the detector. In this way the calibration source can be turned on or off.

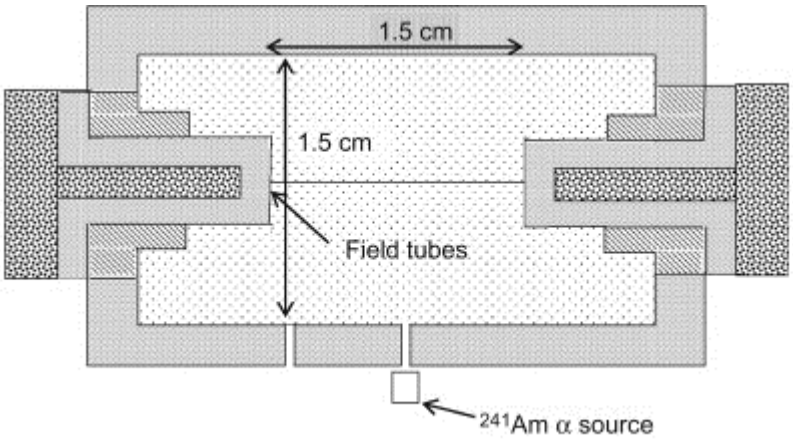

Figure 3.5 Cross sectional of GPC

3.2.2 Tissue Equivalent Gas and Gas Filling System

Propane based tissue equivalent gas was choose for this study. This gas was recommended due to its better gas gain properties than methane based tissue equivalent gas as was shown in chapter two. The propane based tissue equivalent gases has the following composition :55% C_3H_8, 39.6% CO_2 and 5.4% N_2. The elemental composition (percent per weight) of this tissue equivalent gas was presented in Table 2.1.

The counter cavity was filled with the counting gas to a low pressure determined by the tissue equivalent gas density in order to simulate a specified microscopic site in tissue; this was done using a vacuum and gas handling system. The usual procedure for gas filling is, initially, a pump down to $1x10^{-3}$ Torr by using a rotary pump. The counter is then filled to about 100 Torr with tissue equivalent gas and pumped down to $1x10^{-3}$ Torr. This procedure may be repeated if the counter has not been in use for some time. The counter is next filled to the proper pressure for operation. The main components of the gas filling system used for the present experimental work is shown in Figure 3.6 .

Figure 3.6 The vacuum system

3.2.3 Signal Processing Electronics

TEPC and GPC are operated in the pulse mode to record each individual energy deposition event. The output pulse, which is proportional to the charge released in the cavity due to an event, from the anode wire is an electric charge. To process pulse signals from the counters, a pulse height analysis system is required. A traditional analog pulse processing has been employed most commonly for micrdosimetry, but digital pulse processing (DPP) has proved to have a superior performance, with the highest throughput and lowest dead time[43]. In the present work, a commercial digital processing system (Model DP5, Amptek) was employed. In this system, shown in Figure 3.7 and Figure 3.8, a pulse extracted by the charge sensitive preamplifier is directly digitized by a sampling ADC which applies real time digital processing to the signal, detects the peak amplitude, and bins this value in its histogram memory, generating an energy spectrum. The spectrum is then transmitted over the DP5's serial interface to the computer.

The charge sensitive pre-amplifier used in this study was a Canberra-2006. The function of this type of preamplifier is to convert the charge pulse produced by an energy deposition event to a voltage spike. For this reason it will be the first component in the signal processing chain. The input capacitance of the preamplifier must be kept to a minimum in order to reduce the electronic noise. This can be achieved through locating the preamplifier as close as possible to the detector, and the input circuits are designed to match the characteristics of the detector30.

The preamp output signal is the input to the DPP, the analog pre-filter prepares the signal for accurate digitization. The pulses input to the ADC should have the characteristics shown in figure 3.9. The counter signal form is digitized with a digitizing

ADC and latter shaped digitally. The digital pulse shaping contains two parallel signal processing paths, the ‘slow channel’ and the ‘fast channel’. The slow channel which has a long shaping time constant is optimized to obtain accurate pulse heights. A single digital quantity which represents the peak value of each pulse is the output of the slow channel pulse shaper. The slow channel threshold is the equivalent to a low level discriminator (LLD). The fast channel is optimized to detect pulses which overlap in the slow channel and measure the incoming count rate. The fast channel discriminator also functions as an LLD and is used to measure the incoming count rate (ICR) and identifies events which are coincident in the slow channel but are separated in the fast channel. The multichannel analyzer (MCA) operates like a conventional MCA, except that the input is already digitized. It detects the amplitude of the peak of the shaped pulse, using a digital peak detect circuit. If the selection logic indicates that the pulse is valid, then it increments the value stored at a memory location corresponding to the peak amplitude. The MCA supports 256,512,1024,2048,4096 or 8192 channels. The DPP allows 16.7 M counts per channel. Data transfers to the computer via USB, RS232 or Ethernet interface and occur based on approximate real computer time. The Amptek’s ADMCA software provides the access to all the required configurations parameters includes very simple analysis and the ability to save the data in suitable format[44].

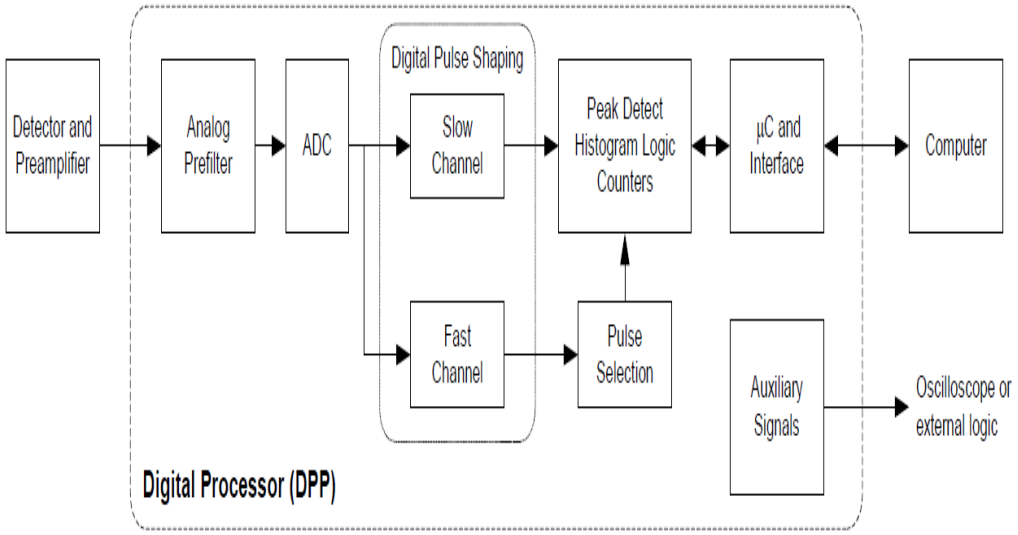

Figure 3.7 Block diagram of the DPP in a complete system

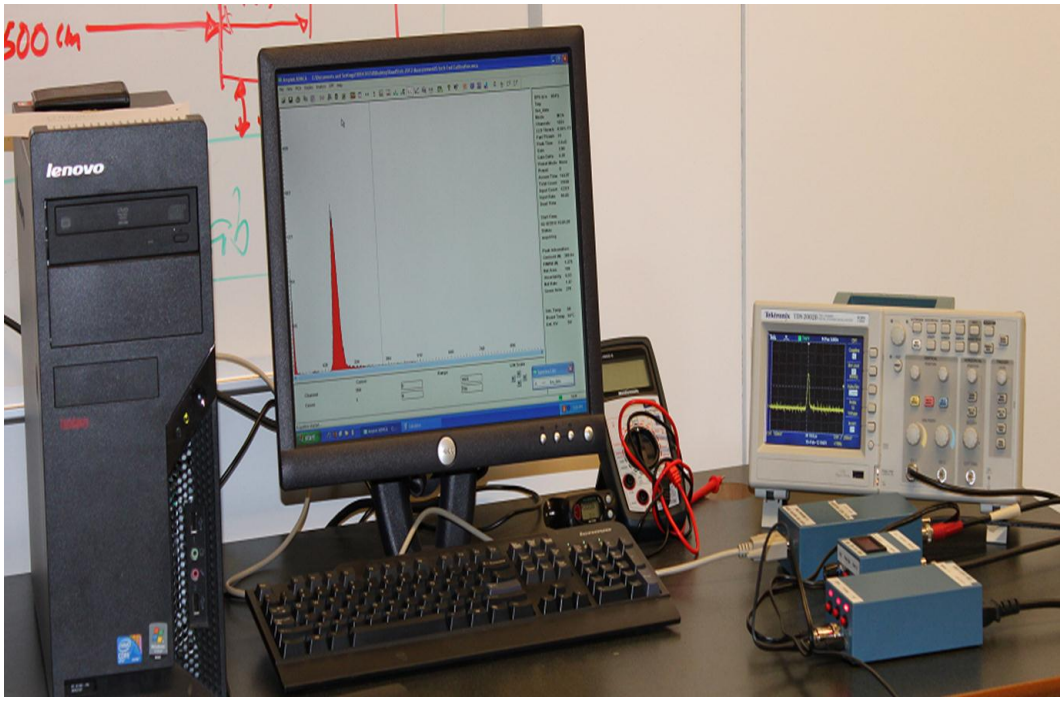

Figure 3.8 the digital pulse processor DPP, high voltage source and power supply unit connected to the computer via USB connection.

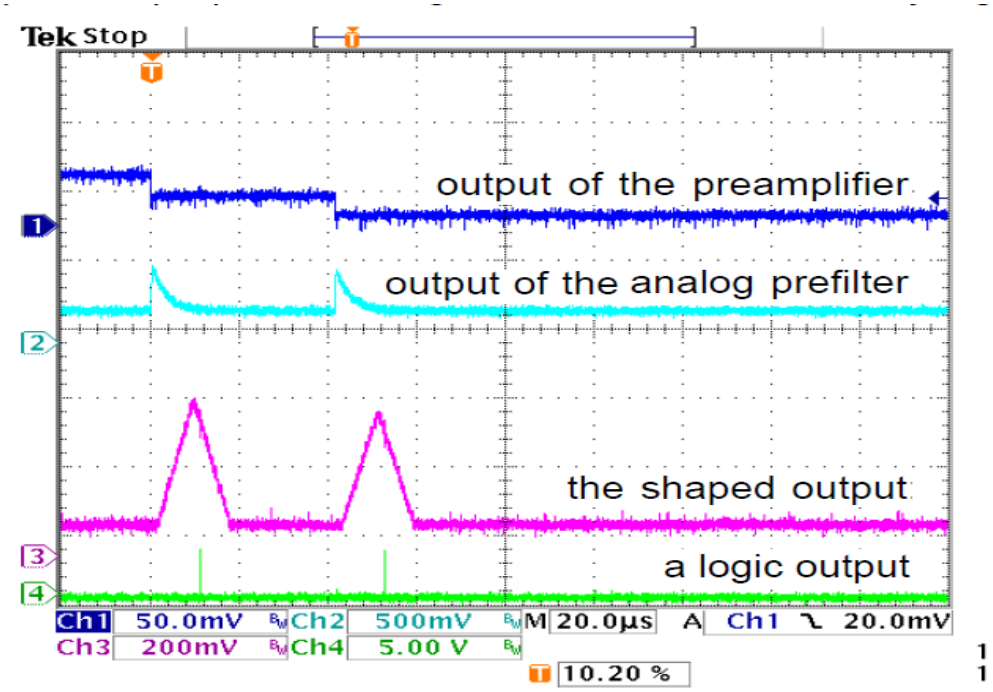

Figure 3.9 Oscilloscope traces illustrating the signal processing.

Figure 3.9 shows the output of the preamplifier, the lower light blue traces show the output of the analog pre-filter, the third lower magenta trace shows the shaped output: it is the peak of these pulses which are detected and binned to form the pulse-height spectrum. The lowest green trace is a logic output indicating that a valid peak has been detected[44].

3.2.4 Calibration Method : TEPC and GPC

The calibration of an instrument is the determination of a calibration factor which is the quotient of the quantity to be measured and the instrument reading obtained under well-defined measuring conditions.

Since low pressure proportional counters are not absolute devices they have to be calibrated in terms of event size. These counters measure pulse rate and pulse height spectra for external radiation, thus such a system is more complex and sensitive to

changes in operational conditions than a detector that uses only pulse rate information such as a Geiger counter.

The goal of calibration of low pressure proportional counters is to convert the counter reading which is the pulse height, h, corresponding to the energy loss of a charged particle and associated secondaries crossing the cavity into energy imparted or the related lineal energy y.

The calibration is generally performed using a built-in collimated source emitting particles of known type and energy. The most common calibration sources in TEPC are ^{244}Cm which emit alpha particles of 5.8 MeV energy; the alpha source in the GPC used in this work was a gold coated Am-241 source (Amersham International) with mean particle energy of 4.35 MeV. Alpha particles are emitted from the source and allowed to pass across the sensitive volume of the counter through a small aperture in the wall. The crossing alpha particles will produce ionisation in the filling gas which is proportional to the amount of energy deposited in the counter. This ionisation is then multiplied by the gas gain of the counter, the resulting charges collected on the anode wire are converted to a voltage pulse and further amplified using preamplifier and linear amplifiers, and then stored in the appropriate channel of a pulse height analyzer. Accordingly pulse height can be converted to lineal energy without knowledge of the absolute gas gain. In practice, as shown in Figure 3.10, as each pulse represents a single energy deposition event, the alpha peak is broadened due to factors such as collimator design and energy straggling. Precise determination of the position of the maximum can be made from fitting the pulse height which representing the energy loss distribution produced by alpha particles from the calibration source to a Gaussian distribution.

The linearity of pulse height versus lineal energy is a factor of some error in measurements, because W values depend on the type and energy of the secondary charged particle, and the value and spatial distribution of gas multiplication cannot be determined accurately. However, such non- linearities are relatively small and have minor influence in practical applications[45].

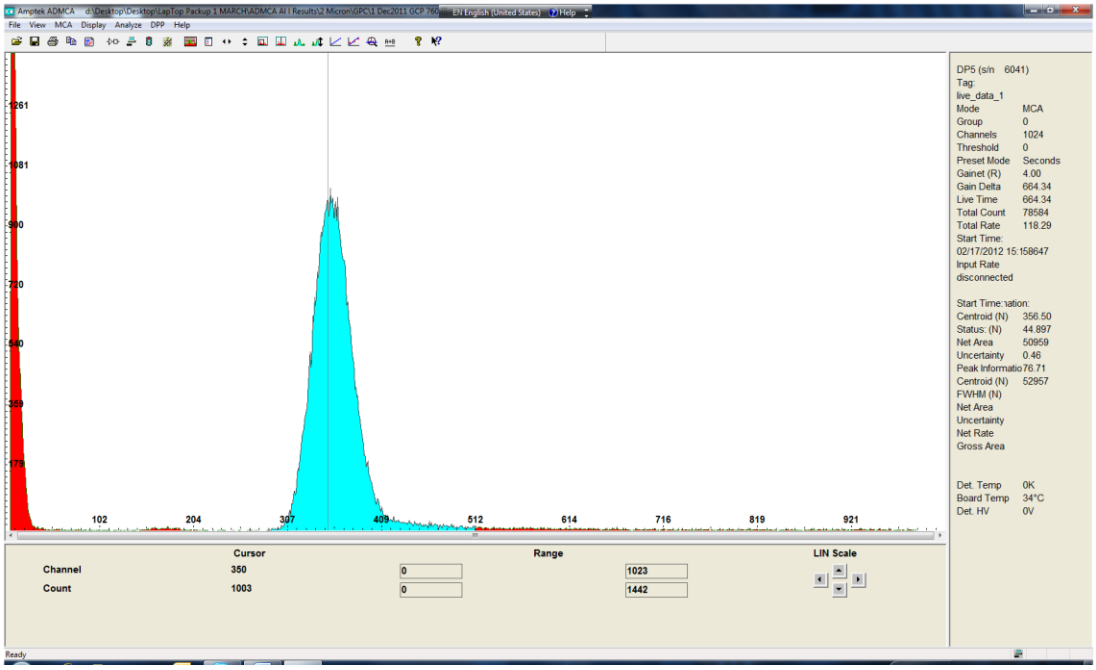

Figure 3.10 Pulse height distribution of internal alpha source for calibration

The channel number corresponding to the middle of the peak indicates the average energy which has been actually lost by the alpha particle crossing the counter. Generally, the mean deposited energy (ΔE) can be calculated by using range-energy data. As an example, the relationship between range and energy of ^{241}Am alpha particles of 4.35 MeV in unit density propane-based Tissue Equivalent gas has been obtained from the Monte Carlo code SRIM (Stopping and Range of Ions in Matter)[36] and is shown for in

Figure 3.11. According to this graph the range corresponds to the mean energy of the alpha particles coming from the source are (28.675 µm).

Since the range of the alpha particles emitted from the source is known (28.675 µm), therefore by reading off the change with regards to energy which corresponds to the difference in range, between (28.675 µm) and (28.675 µm - d µm), where 'd' is the simulated site diameter , the energy deposition of the alpha particles (ΔE) which cross any simulated diameter can be found. The energy deposition due to ^{244}Cm and ^{241}Am calibration source for the range of simulated site diameter used in this study, is given in Table 3.3.

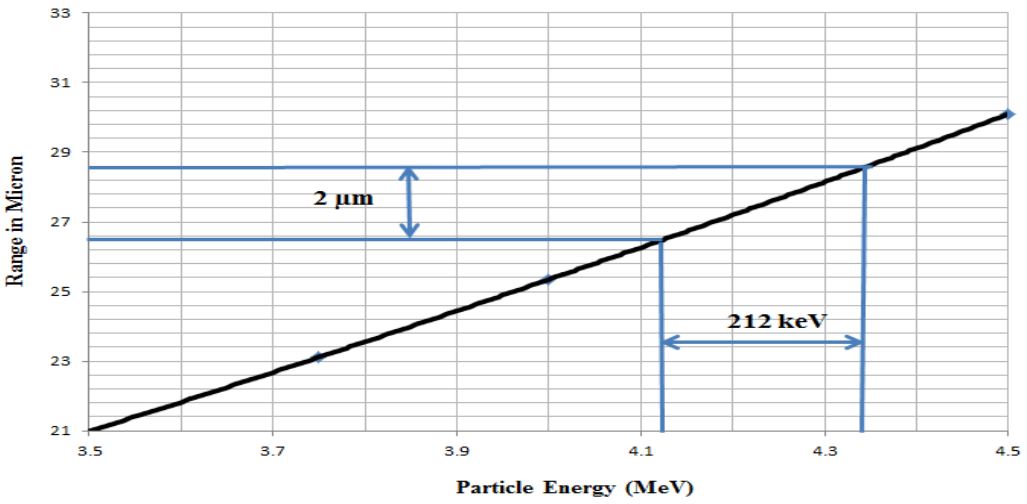

Figure 3.11 Ranges Versus Energy Relationship of ^{241}Am Alpha Particles in Tissue.

Simulated Diameter (µm)	Energy Deposition of ^{244}Cm (keV)	Energy Deposition of ^{241}Am (keV)
2	169	212
4	348	431.8
8	715	897.4

Table 3.3 Energy Deposition Due To ^{244}Cm and ^{241}Am Particles For Various Site Diameter.

To obtain a calibration factor (CF) necessary for the conversion of the MCA channels into lineal energy, the 'y' value calculated from energy loss of alpha particles is divided by (h_c), the channel number of the alpha particle energy loss peak observed on the multichannel analyzer. Thus a calibration factor is obtained in terms of keV/µm/Channel Number:

$$\text{CF} = \frac{y}{\text{hc}} = \frac{\Delta E/\bar{l}}{h_c} \qquad (3.2)$$

If two amplifiers with different gain need to be used, the gain ratio needs to be introduce in the equation of the second calibration factor.

The sharp cutoff 'edges' of the pulse height for protons released by neutron interactions, which is 130 keV/µm for 2 µm site size, can also be used as an internal calibration value[46].

The method used to redraw the events frequency as function of lineal energy is show in Figure 3.12. The main graph presents the distribution of events frequency as function of channel number. Each Pulse height multiplied by the calibration factor will produce the corresponding value of lineal energy 'y'. The right upper graph showing the way the events frequency will appears as function of lineal energy. In the example shown for a TEPC simulating a 2µm site size, the value of the channel number of the alpha particle energy loss peak (h_c) was 178. The calibration factor will be :

$$\text{CF} = \frac{y}{\text{hc}} = 127/178 = 0.715 \quad \text{keV/µm/channel}$$

If the calibration factor is multiplied by the lowest channel on the MCA (5) and also by the last multichannel analyzer channel number (1024), the lowest measurable event size and the highest event size for the spectrum can be determined. In this case the maximum and minimum values of the event size are:

$$3.575 \text{ keV/µm} \leq y \leq 723.160 \text{ keV/µm}$$

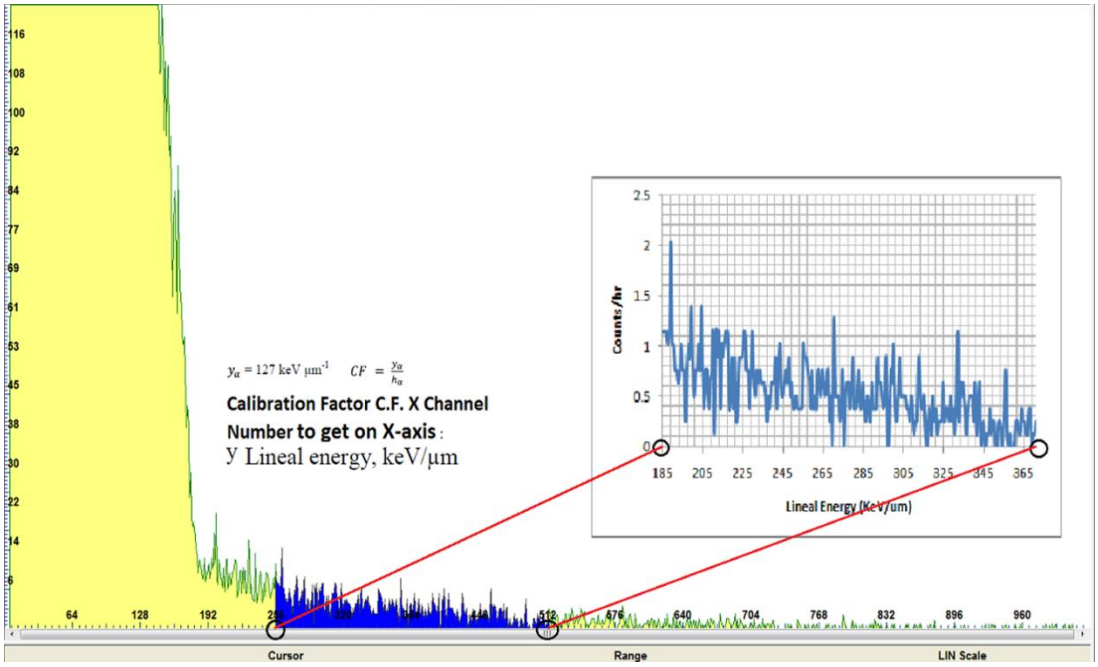

Figure 3.12 Screen shoot from the MCA output with an explanation graph showing the method to change the channel number to lineal energy for events between channel 256 to 512.

For the GPC used in this study, the calibration procedure is different slightly, because the GPC has field tubes that can be independently adjusted to provide a uniform gas gain along the length of the anode wire and define a sensitive cylindrical volume of 1.5 cm length and diameter. This counter was so designed that the ^{241}Am calibration source can be moved from a position in which the alpha particles traverse the centre of

the sensitive volume to a position corresponding to the end of a field tube. The field tube voltage is adjusted so that the pulse height spectrum from the calibration source agrees with the central position measurement indicating uniform gas gain along the central wire. Theoretically, the optimum field tube voltage has been found to be about 23% of the wire voltage, but practically we found it to be about 25% of anode voltage. Figure 3.13 show the pulse height spectrum at centre (the shadow green spectrum) and the pulse height spectrum at end (the blue solid-line spectrum).

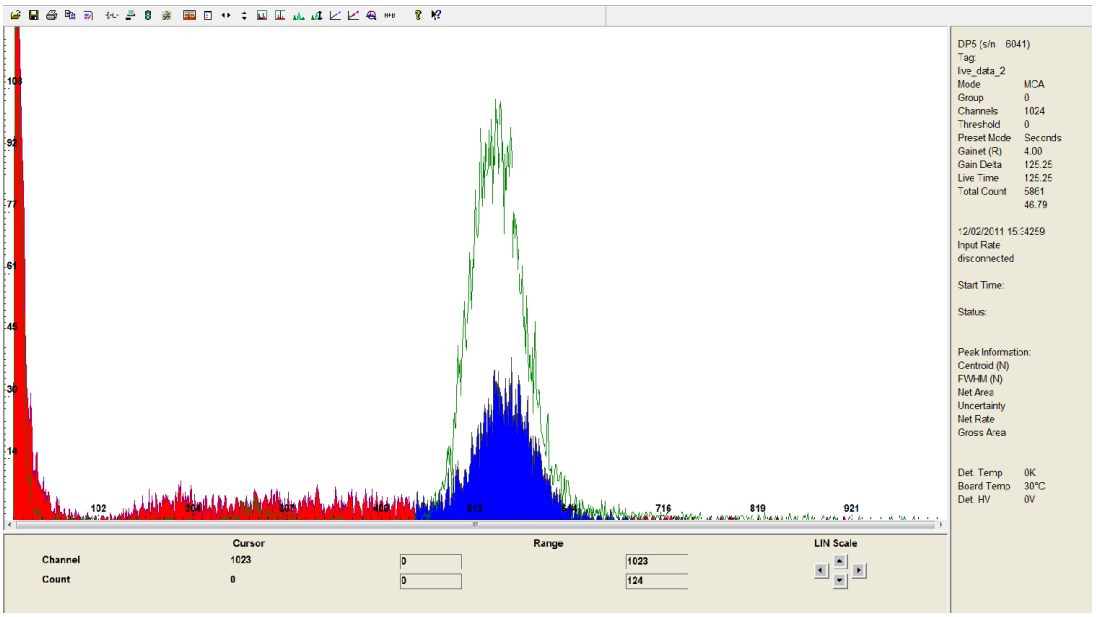

Figure 3.13 The pulse height spectrum at centre (the shadow spectrum) and the pulse height spectrum at end (the blue spectrum).

3.3 The Procedure of Measurement and Equipment preparation

Prior to being connected to the electronic system and the rest of the instrumental set-up, the counters were prepared for the experiment. In order to simulate a defined site size, the counter would undergo the processes of evacuating and filling with a gas to the

desired pressure, as discussed before. In the case of experiments reported in this work, only one spectra were required to cover the whole lineal energy range of interest (between 3 keV/µm and 750 keV/µm). After calibration of the counter and finding a suitable gain setting and operating high voltage (and field voltage for GPC), the counter is placed in its position and the experiment is run to collect the pulse-height spectrum.

The Am-Be source of the UOIT facility has a relatively low emission rate. So in order to minimize the inherent counting statistics, we needed to accumulate enough counts per channel with a prolonged measurement. A single run was extended for more than 24 hours in most of the cases. However, the longer the measurement duration, the more likely there is to be drift of the gas gain. By repeating the calibration of the counter before and after the measurement, it could be checked that the gas gain had not drifted during the measurement. Less than $\pm$1% variation was noticed as a maximum drift in all the measurements.

3.4 Presentation of Microdosimetric Event-Size Spectra

3.4.1 Event-Size redistribution technique

The linear representation for the raw measurement data, which is the number of times an event occurs as function of the size of the event itself, measured in terms of lineal energy, is not particularly useful for a clear interpretation of the data. As shown in step a of Figure 3.14, events can occur over a wide range of sizes from about 1 keV/µm to 1000 keV/µm, which means more than three decades of lineal energy. To improve the presentation of the data and to aid its interpretation, this raw information is modified by redistributing the data onto a scale constructed of 50 equal logarithmic intervals or bins

per decade of lineal energy. The redistribution of the event-size data is achieved in the following manner.

First, to create a smoother plot the 1024 lineal energy bins are subdivided by a factor of 25 such that the contents of each of the 1024 channels are evenly divided into the 25 sub-division, thus producing an array of (1024X25) lineal energy bins contains the frequency of events.

Second, by using the formula: $y(i) = 10^{X/50}$, the required logarithmic intervals can be created. Where X represents an index of the logarithmic bin number as shown in figure 3.15. As an example, if lineal energy bins for the five decades between 0.01 to 1000 keV/µm is to be represented, we begin with X= -100 which represents a linear energy value of y = 0.01 keV/µm. By increasing X in increments of 1 to reach -50, a lineal energy value of y = 0.1 keV/µm will be reached. This process can be continued to construct the entire logarithmic scale from 0.01 to 1000 keV/µm.

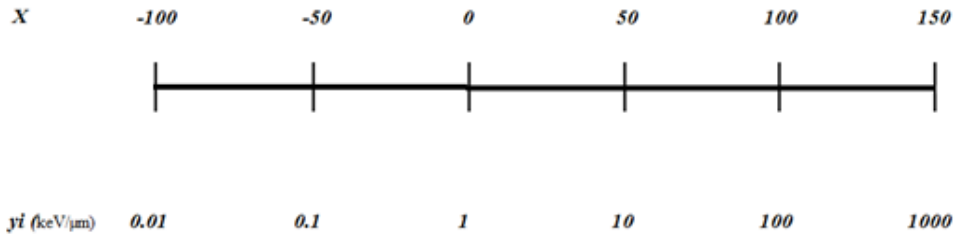

Figure 3.15 Equal logarithmic intervals creation procedure.

Third, to transfer the contents of the (1024X25) linear scale of event frequency to the new logarithm scale of lineal energy we proceed as follows. The upper value of the first logarithmic bin is used to determine its position on the linear scale and the events up

to that value are summed and transferred to the logarithmic bin. This process is continued logarithmic bin by logarithmic bin until all the frequency data has be transferred onto the logarithmic scale shown in b of figure 3.14 .

The construction of the 150 new equal logarithmic interval bins for the lineal energy distribution was created with a program built in MATLAB (see Annex I). The basic mathematical idea behind the creation of new bins width is that the relationship between the logarithmic value and the linear value for an event-size interval is given by:

$$d\,Ln(y)/dy = 1/y \qquad (3.3)$$

Where 'd Ln(y)', is the interval between the geometrical centres of two consecutive increment (y_i - 1/2 and y_i + 1/2). The linear interval 'dy' is given by : dy = (y + dy) – y.

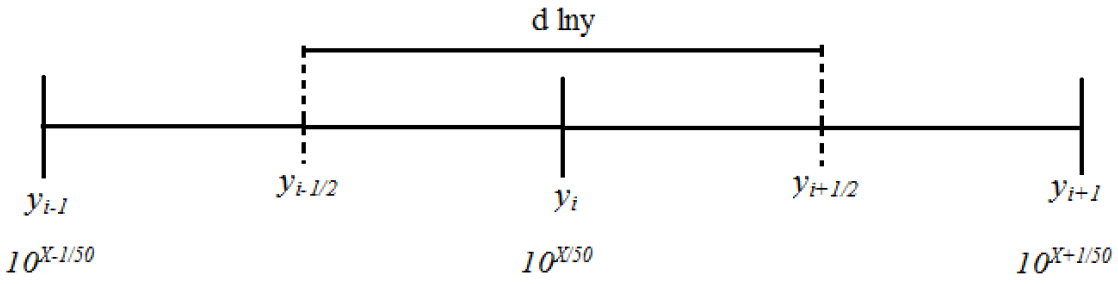

Figure 3.16 Example of two bins along the logarithmic lineal energy axis.

The change in the lineal energy from a bin centre to another is mathematically represents as:

$$dy = [(y_i+1/2) - (y_i-1/2)] = [\,10^{(X+1/2)/50} - 10^{(X-1/2)/50}]$$

$$dy = 10^{(X/50)}[10^{(1/100)}-10^{-(1/100)}] \qquad (3.4)$$

Substituting equation 3.4 into equation 3.3 yields:

$$d\,Ln(y) = 10^{(X/50)}[10^{(1/100)}-10^{-(1/100)}] / 10^{(X/50)} = 10^{(1/100)}-10^{-(1/100)}$$

$$d\,Ln(y) = 0.046055 \qquad (3.5)$$

The d Ln(y) term represents how far apart are the logarithmic lineal energy points shown in Figure 3.16 are and such a distance is centred about y_i linear lineal energy point; also note that geometrically speaking, this distance is equal to the width of a logarithmic lineal energy bin. This term is the normalizing factor used in the numerical evaluation of both the frequency and dose distribution of event-size. This is the same as that derived and recommended in Appendix "B" of ICRU Report 36[19].

The improvement of data presentation can be shown clearly by monitoring the change of the graph shape as shown in Figure 3.14b, where the frequency spectrum of figure 3.14a logarithmically redistributed onto a 50 equal logarithmic intervals of lineal energy. The ordinate gives the total number of counts in each logarithmic interval registered during the measurement. The vertical height of the spectrum therefore depends on the total number of counts recorded, which for a constant radiation field, would depend on the total measurement time.

It is clearly shown in figure 3.14b representation of the data, that large events are typically rare, because data above 150 keV/μm often have a few channels with one count and many zero. Some further work towards a normalised dose distribution needs to be done to reach the final step c in figure 3.14, as will be discussed later.

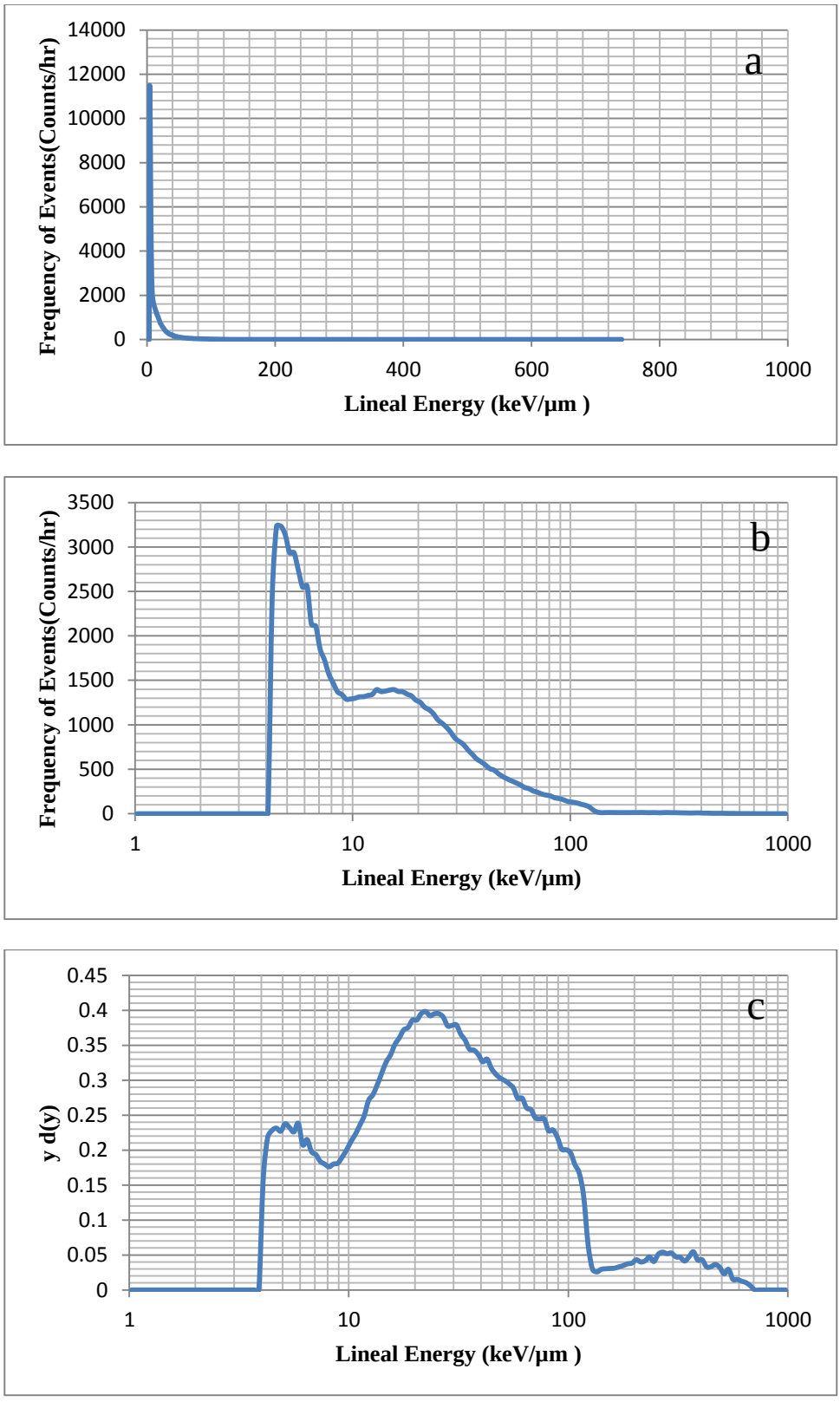

Figure 3.14. The improvement of data presentation can be shown clearly by monitoring the change of the graph shape through Step a, step b and c.

3.4.2 Frequency Distribution: Mathematical Description and Normalization

Generally f(y) refers to the number of events occurring between event sizes ‘y’ and ‘y+dy’, where dy= (y+dy) – y. Mathematically speaking, since the frequency distribution is in fact a probability density of ‘y’ it can be normalized to unity in terms of a linear scale by definition:

$$\int_0^\infty f(y)\, dy = 1.0 \qquad (3.6)$$

On a linear scale then equal areas represent equal probabilities. For all the spectra obtained in this work, however, logarithmic scales of event size ‘y’ have been employed to represent the various distributions. In other words ‘dy’ which is a linear interval is replaced by ‘dLny’ which is a logarithmic interval. Each decade of linear energy has been subdivided into equal logarithmic intervals. In the case of the normalised frequency distribution based on logarithmic scales the following expressions are valid:

$$dy = y.\, d\,(\mathrm{Ln}\, y) \qquad (3.7)$$

Therefore :

$$\int_0^\infty f(y)\, dy = \int_0^\infty y\,.\, f(y).\, d\,\mathrm{Ln}y = 1.0 \qquad (3.8)$$

The way in which is this done is each bin frequency is normalised by the following operation :

$$f(y_i) = [f(y_i) \;/ \sum_{i=0}^{150} f(y_i)] \,.\, (1/d\,\mathrm{Ln}(y)) \qquad (3.9)$$

Such that :

$$\sum_{i=0}^{150} f(y_i) \,.\, d\,Ln(y) \quad = 1.0 \qquad (3.10)$$

Where:

$f_{n,i}$ = normalised frequency of the i^{th} bin

f_i = frequency of the i^{th} bin

n = total number of bins

d $Ln(y_i)$ = logarithmic lineal energy bin width and equal 0.046 according to equation (3.5)

3.4.3 Dose Distribution: Mathematical Description and Normalization

It is not the frequency at which events of a given size occur that is of interest but the fraction of the total absorbed radiation energy which is deposited by the events of a given size. Thus a second modification that is made with the raw data is the calculation from the frequency distribution to a dose distribution representing the fraction of the absorbed dose deposited by events within a specified event-size range. 'y.f(y)' represents the dose distribution d(y), which is the total amount of kinetic energy deposited in the gas cavity by the associated charged particles.

The dose distribution d(y) is a probability density which can be normalised to unity by the expression:

$$\int_0^{\infty} y \,.\, d(y)\, dy = 1.0 \qquad (3.11)$$

The linear representation of a normalised dose distribution can be expressed as:

$$\int_0^\infty y \,.\, f(y)\, dy = \int_0^\infty d(y)\, dy = 1.0 \qquad (3.12)$$

Here again equal areas represent equal dose fractions. Referring to the equation (3.7), the logarithmic representation of the dose distributions normalized to unit area is expressed as:

$$\int_0^\infty y.\, f(y)\, dy = \int_0^\infty y^2 f(y)\, dLny = 1.0 \qquad (3.13)$$

Or

$$\int_0^\infty y\, d(y)\, dlny = 1.0 \qquad (3.14)$$

Part c of Figure 3.14 shows an example of the normalised microdosimetric distribution y.d(y) plotted as a function of 'y' on a logarithmic scale for Am-Be with 2 µm simulated diameter. The value of yd(y) for each bin is given by the following equation:

$$y_i \,.\, f(y_i) = [y_i.f(y_i) \;/ \textstyle\sum_{i=0}^{150} y_i \;.\, f(y_i)]\; (1/d\, Ln(y)) \qquad (3.15)$$

Such that :

$$\textstyle\sum_{i=0}^{150} y_i \;.\, f(y_i) \,.\, d\, Ln(y) = 1.0 \qquad (3.16)$$

Where:

y_i = mid-point of the i^{th} lineal energy bin

f_i = frequency of the i^{th} lineal energy bin

n = total number of bins

d Ln(y) = logarithmic lineal energy bin width and equal 0.046 according to equation (3.5)

3.5 The Calculation of Total Dose and Dose Equivalent from Measured Event-Size Spectra

The total deposited energy (absorbed dose) in the gas cavity can be obtained by summing up the energy deposited by each individual event. If the whole counter, cavity and wall, is considered as a homogenous tissue equivalent device then the absorbed dose in tissue can be derived by integration over the measured event-size spectrum and the application of a constant which takes into account the cavity dimensions, and the conversion of lineal energy in keV/μm into imparted energy in joules.

The absorbed dose in a microdosimetric tissue volume D_t is the same as that simulated by a low pressure gas cavity of diameter d_d and is given by :

$$(\text{Dose})_{\text{tissue}} = (\text{Dose})_{\text{gas cavity}} = \text{Energy Absorbed (J) / Mass of Gas (kg)}$$

$$D_d = \frac{\varepsilon_d}{m_d} = \bar{l} \cdot \frac{\sum_{i=0}^{\infty} y_i . f(y_i)}{m_d} \qquad (3.17)$$

Where $\bar{l}$ = 2/3 d_t is the mean chord length of the simulated tissue in micron, $\sum_{i=0}^{\infty} y_i . f(y_i)$ is the product of event-size y_i and the number of times the event occurs over the entire spectrum of event-sizes. The mass of the gas m_d depends on the geometry of the counter and is calculated for spherical detector cavity as follows:

$$m_d = \rho_g . \pi/6 . d_d^3 \qquad (3.18)$$

Rearrange equation (3.17) will give:

$$D_d = \sum_{i=0}^{\infty} y_i . f(y_i) \ . 4. d_t \ / \ (\rho_g . \ \pi . d_d^3) \qquad (3.19)$$

From equation 2.17 it was shown that ρ_g is equal to $\rho_t . d_t/d_d$, and to convert the absorbed dose from keV/kg to Gray, equation (3.17) should be multiplied by $1.6 * 10^{-16}$ Joule/keV, and will be:

$$D_d = \frac{4}{\pi} . 1.6 . 10^{-16} . \frac{1}{\rho_t} . \frac{1}{d_d^2} \sum_{i=0}^{\infty} y_i . f(y_i) \qquad (3.20)$$

Accordingly :

For 12.9 cm (5 inch) TEPC, Absorbed Dose = $1.2258*10^{-5}$ * ($\sum_{i=0}^{\infty}$ yi. f(yi))

For 5.1 cm (2 inch) TEPC, Absorbed Dose = $7.8431*10^{-5}$ * ($\sum_{i=0}^{\infty}$ yi. f(yi))

For 1.5 cm GPC, Absorbed Dose = $9.066*10^{-4}$ * ($\sum_{i=0}^{\infty}$ yi. f(yi))

Equation 2.5 and 2.6 for the mean $\bar{y}_F$ and $\bar{y}_D$ can be rewritten as summation expressions as follow:

$$\bar{y}_F = \sum_{i=0}^{\infty} yi. f(yi) \ / \ \sum_{i=0}^{\infty} f(yi) \qquad (3.21)$$

$$\bar{y}_D = \sum_{i=0}^{\infty} yi\text{^}2. f(yi) \ / \ \sum_{i=0}^{\infty} yi. f(yi) \qquad (3.22)$$

TEPCs are commonly used to determine the dose equivalent H by calculating the average quality factor $\bar{Q}$:

$$H = \int Q(y) D(y) dy \qquad (3.23)$$

$$H = \bar{Q}.D \qquad (3.24)$$

Q(y) can be chosen numerically equal to the quality factor Q(L) which defined by ICRP-60[3] as:

$$\mathbf{Q(L)} = \begin{cases} \mathbf{1} & \boldsymbol{L < 10\ keV/\mu m} \\ \mathbf{0.32L - 2.2} & \mathbf{10 < L < 100\ keV/\mu m} \\ \frac{\mathbf{300}}{\sqrt{\boldsymbol{L}}} & \boldsymbol{L > 100\ keV/\mu m} \end{cases}$$

There is no change in quality factor formula between ICRP-60 and ICRP-74 for neutron of energy more than 1MeV.

Average quality factor $\bar{Q}$ can be calculated by using summation expressions as follow:

$$\bar{Q} = \sum_{i=0}^{\infty} Q(yi).yi.f(yi) \,/\, \sum_{i=0}^{\infty} yi.f(yi) \qquad (3.25)$$

The quality factor by ICRP is given as function of Unrestricted Linear Energy Transfer and assumes that the lineal energy of a secondary charged particle that traverses the gas cavity is equal to this unrestricted linear energy transfer. This is not completely true since the lineal energy of such a particle will fluctuate about it actual unrestricted linear energy transfer and lineal energy is a restricted quantity determined by the size of the simulated volume.

3.6 Discrimination between Neutron and Gamma Absorbed Dose

In radiation protection as well as in dosimetry for radiation therapy and radiobiology it is usually required to determine the dose contributions from photons and neutrons separately. The TEPC alone or accompanied with GPC can be used to distinguish photon and neutron dose contributions with good accuracy. The standard

method is based on the fact that secondary particles from interactions of photons (electrons) and neutrons (protons and heavier particles) with tissue equivalent gas and tissue equivalent-wall or graphite walled contribute to different parts of the y spectrum. There are parts in the y spectrum where the two contributions overlap and difficult to be discriminated, mainly between 1 and 10 keV/µm. The accuracy of the separation depends on the extent of the overlap and the knowledge of the shapes of the photon and neutron y spectra in this region.

Independently of their energy, photon contribute up to about y= 10 keV/µm. The position of this 'electron edge' is determined by the maximum energy loss of secondary electrons along a given path length and depends, therefore, on the simulated diameter. For photon energies in the 10-100 keV regions, as it is the case in this study, the shape of the measured distributions varies significantly with energy. Photoelectric effects are the dominant interaction process for photons of an average energy less than 20 keV and dose is delivered almost completely by photoelectrons. Microdosimetric spectra become broader due to an increasing contribution of crossers as energy increases upward from 20 keV, and any Compton electrons are totally absorbed in the sensitive volume. Photoelectrons contributions to dose began to decrease and contributions due to Compton electrons begin to increase as photon energy increase. 91% of the dose fraction is still produced by photoelectrons at 33 keV photons, and become 8% by photons of average energy 118 keV[47]. Thus, at 60 keV, we expect that Compton electrons of average energy of 9.2 keV to be the major contributors of the dose fraction deliver to the site. Electrons of average energy 9.2 keV have a range of approximately 2 µm, the same as the site diameter. Accordingly should give rise to a spectrum of event-sizes having a very

dominant shoulder region. The dose contribution by neutrons below 1 keV/μm is generally very small and depends in a complex way on the neutron energy[13]. The shape of the y spectra by neutrons in the MeV range (appears below 10 keV/μm) will change significantly as a function of neutron energy due to the significant influence by energy loss straggling of high energy recoil protons[45].

Three different techniques for unfolding photon and neutron events have been applied in this work:

(1) The determination of the minimum between the two regions in the yd(y) and the assumption that events which are to the left of that point (less energetic) are due to photon interactions and events to the right of that point (more energetic) are due to neutrons;

(2) The fitting of a previously stored spectrum of events due to photon interactions in the counter wall;

(3) Two counters with different sensitivity for different radiation components.

3.7 Uncertainties in Experimental Microdosimetry

Uncertainties based on counting statistics in the average of lineal energy distributions and the quality factor can be obtained using the error propagation formulae[30]. The formulae for calculation are shown below and the results are listed in Table 4.2.

$$\sigma_{\bar{y}F}/\bar{y}_F = \sqrt{\frac{1}{\sum_{i=1}^{N} f(yi)} + \frac{1}{\sum_{i=1}^{N} d(yi)}} \qquad (3.26)$$

$$\sigma_{\bar{y}D}/\bar{y}_D = \sqrt{\frac{\sum_{i=1}^{N} y^2\, d(yi)}{[\sum_{i=1}^{N} yi\, d(yi)]\text{^}2} + \frac{1}{\sum_{i=1}^{N} d(yi)}} \quad (3.27)$$

$$\sigma_Q/\bar{Q} = \sqrt{\frac{\sum Q(yi)^2 d(yi)}{[\sum_{i=1}^{N} Q(yi) d(yi)]\text{^}2} + \frac{1}{\sum_{i=1}^{N} d(yi)}} \quad (3.28)$$

3.7.1 A Discussion of the source of Uncertainty

The estimation of the level of the errors or uncertainities in microdosimetric practices is important as it is with any experiment both for errors systematic and statistical in nature.

Experimentally induced uncertainities are mostly produced in connection with the electronics and other related measuring equipment. Such as the correct setting of the amplifier gains for calibration and measurement. On the other hand, uncertainities may be introduced by the measurement procedure itself, for example, gas filling and calibration of the proportional counter. In particular the question of the correct W-value for the radiation field being measured, compared to that of the alpha particles used for calibration is most important. Another possible source of error is related to the manipulation of the raw data in data analysis. The stochastic nature of energy deposition events by charged particles in the sensitive volume of the counter, introduces yet another source of error. The size of errors depends also on how long the measurement is made. For the work reported here the statistical uncertainity of the spectrum averages such as 'y_D' and 'y_F' were always less than 1%. With regards to the calculation of absorbed dose, it would

appear that calibration and W-value problems introduce the largest degree of uncertainity and that the absorbed dose values reported here have an associated uncertainity of ($\pm$4.8%). The gas gain was found to be stable within 2.5% over periods in excess of twenty-four hours.

Chapter Four : Results and Discussion

As was indicated in the first chapter, one of the major factors regarding the radiation exposure to workers in nuclear facilities is due to radiation fields of mixed nature, especially neutron and gamma fields. Therefore the need for improving the method of mixed field dosimetry in all energy regions is important. Thus a general study in applying microdosimetric techniques to Am-Be neutron source with average neutron energy in the MeV region was the main motivation of this research.

What is discussed and analyzed in this chapter is based on the valuable information obtained regarding the mixed radiation field by changing the counter gas pressure and making measurements with gas cavities simulating unit density, microscopic volumes of 2 μm to 8 μm diameter. The absorbed dose to the gas cavity is determined through the individual energy deposition events of secondaries produced by the interaction of neutrons and gamma with the counters. The amount of absorbed dose to the gas cavity is of course determined by the nature of the material surrounding the cavity and the gas cavity itself, this is the essence of cavity theory.

Each microdosimetric event-size spectrum was measured by recording the pulse height spectrum as described before. The accumulated raw data was then transferred to the computer, and saved as a complete frequency and dose distribution with the raw data redistributed on a logarithmic scale of event size. For all the measurements the output of the source was constant and the source detector geometry fixed or corrected. The microdosimetric data analysis programme caries out a normalisation of the frequency and dose distribution such that the area under the frequency distribution curve presents a

probability of 1.0, and the area under the dose distribution curve represents unit absorbed dose. The most concise way to present the microdosimetric data is to tabulate $\bar{y}_F$, the frequency mean lineal energy and $\bar{y}_D$, the dose mean lineal energy for the entire range of measured radiation energies and site sizes and to measure the absorbed dose, dose equivalent and mean quality factor. More complete information can be obtained from the plot of yd(y) as a function of lineal energy y, where the area delimited by any two values of lineal energy y, is equal to the fraction of dose delivered in that interval.

4.1 Tissue Equivalent Proportional Counter Measurements

4.1.1. Examination of the Performance of the Tissue Equivalent Proportional Counters:

An assessment of the performance of three tissue equivalent proportional counters under identical radiation field conditions has been done through measuring microdosimetric event-size spectra for neutrons produced by the Am-Be neutron source. Proportional counters obtained from Far West Technology have been used in this investigation. Two of the three counters were 5" diameter Model LET-SW5 counters and the third was a 2" diameter counter Model LET-SW2. The resolution of both types counter is not significantly different.

Figure 4.1 shows the microdosimetric event-size spectra measured in the same position of the radiation for the three proportional counters and Table 4.1 list of spectrum parameters. The general shape of the spectra is what would be expected for Am-Be neutron energy spectrum. The dominant feature is the peak between 10 keV/µm and 130 keV/µm with a maximum at around 26 keV/µm. This peak arises from the interaction recoil protons and is known as the proton peak. The sharp edge on the high lineal energy

side of this peak termed the proton 'edge' is due to the fact that recoil protons with an energy corresponding to their maximum stopping power and crossing the spherical volume along a diameter deposit the maximum amount of energy possible for a proton interacting with the simulated tissue volume, in this case 2 μm in diameter. The more recoil protons present per unit dose in the radiation field having energies around the maximum in the stopping power curve i.e. ~ 100 keV then the greater will be the drop at the edge. The position of the proton edge is of course a constant for all neutron radiation fields for a given simulated diameter. From Figure 4.1 and Table 4.1, it appears that there is excellent agreement between the three event-size spectra and the proton edges appear at the same position on the lineal energy scale and the differences in microdosimetric parameters $\bar{y}_D$ and $\bar{y}_F$ are not exceeding 3%. Any difference in the values, may be due to the accuracy of the cavity pressure and the calibration process by internal α sources only. At around 130 keV/μm the calibration with alpha particles is assumed linear over the entire range of event sizes from approximately 0.2 keV/μm to 1000 keV/μm, this point has been investigated by Herskind using characteristic X-rays as well as alpha particles for calibration and found to be case within 3-5%.[46] The differences in W-values between α particles and the rest of the charge particles which interact with the counters to place an event size spectrum will not be taken into consideration, although the absolute value of the spectral parameters will of course be affected by W-value differences, because the correction will be the same for each counter. According to the literature this difference was estimated to result in a decrease of 3% in both $\bar{y}_D$ and $\bar{y}_F$ for low energy neutron measurements with counters calibrated with alpha particles.

Proportional Counter	$\bar{y}_F$	$\bar{y}_D$	Av. Quality Factor Q
2″ - 1181	20.70	52.80	9.80
5″- 1230	21.82	53.49	9.82
5″- 1236	20.55	52.21	9.70
Mean Value	21.02	52.83	9.77
Coefficient of variation	3.02%	1.21%	0.6%

Table 4.1 microdosimetric parameters determined from measurements with three different proportional counters simulating spherical volumes of 2 μm diameter and irradiated with Am-Be neutron source.

Experimental uncertainities in microdosimetric measurements is shown in table 4.2, which gives an assessment of the change in microdosimetric parameters due to measurement uncertainties. An estimation of the statistical fluctuations was made by calculating the event-size spectrum moments with data representing the extremes of the counting statistics, the value of $\bar{y}_F$, $\bar{y}_D$ and average quality factor Q shown in table 4.2 indicate differences of 4.8%, 0.7% and 3% respectively. Counting statistics therefore account for the greatest uncertainty in the measuring procedure and as the above values are extreme limits they represent a reasonable estimate of the overall uncertainty in the values of frequency mean and dose mean.

Proportional Counter	$\bar{y}_F$	$\bar{y}_D$	Av.Quality Factor Q
2" - Rossi	20.70	52.80	9.80
Counting statistics σ	$\pm$0.5	$\pm$0.20	$\pm$0.16

Table 4.2 Assessment of change in microdosimetric parameters due to measurement uncertainties

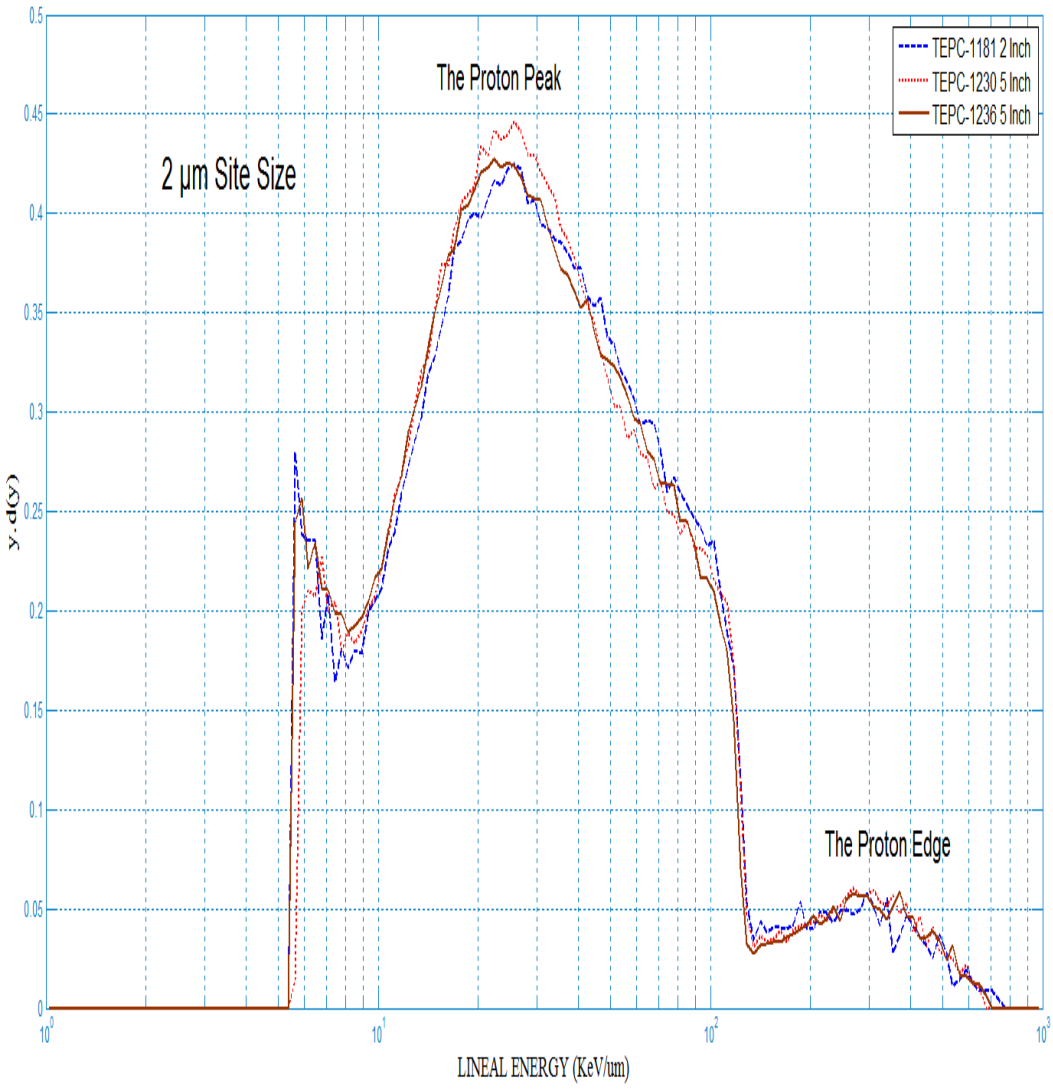

Figure 4.1 Linear energy event-size spectra measured with three Tissue Equivalent Proportional Counters.

4.1.2 Dose Rates and Dose Equivalent for Mixed Field Photons and Neutrons from an Am-Be Neutron Source

The lineal energy distribution as shown in Figure 4.2 have three components, below 10 keV/µm, between 10 and 130 keV/µm and above 130 keV/µm . Table 4.3 shows that

there are about 24500 events per hour as an average of the first component, below 10 keV/μm, which is composed mainly of electron events caused by external photons generating in the Am-Be Source and internal photons generating in the A-150 plastic, about 30000 events are the second component between about 10 and 130 keV/μm corresponding to recoil protons generated in the A-150 plastic, and around 299 events represent greater than 130 keV/μm which is due to α particles and recoil nuclei.

Table 4.3 gives the values of $\bar{y}_D$, $\bar{y}_F$, and $\bar{Q}$ for different tissue sizes using different TEPC counters obtained after the subtraction of γ rays. It is interesting to note that our measurement results compare well to those obtained by others using the same standard TEPC and the Rossi-type, TE spherical wall-less counter filled with propane based TE gas. For example, at a neutron energy between 1.5 MeV and 6 MeV , Srdoc and Marino[13] obtained a $\bar{y}_D$ range between 57.7 and 48.3 with the wall-less Rossi-type counter simulating 2 μm tissue site , which agrees to a great extent with the $\bar{y}_D$ obtained in this study for the same tissue site diameter as shown in table 4.4. The $\bar{y}_F$ values also compare well. A further comparison of $\bar{y}_D$ with that of Srdoc and Marino at the same energy range for simulated diameter of 4 μm also confirms the agreement between two sets of separate measurements. The $\bar{y}_D$ and $\bar{y}_F$ values obtained in this study for a 3 μm simulated diameter also compare well within the variance range of those obtained by Nunomiya et.al.[48] with the same simulated site size using a 5" spherical TEPC as shown in table 4.5.

Site Size (μm)	Counter Type	Total Events	Proton Events	α & heavy Particles	$\bar{y}_F$	$\bar{y}_D$	$\bar{Q}$	D,Absorbed Dose (μGy/hr)	H,Equivalent Dose (μSv/hr)
2	5"-1236	63588.00	32556.00	316.00	20.55	52.21	9.70	16.01	155.30
2	5"-1230	49460.00	31802.00	290.00	21.82	53.49	9.82	13.70	134.53
2	2"-1181	62981.00	34119.00	293.00	20.70	52.80	9.80	14.23	139.45
Average		58676.33	32825.67	299.67	21.02	52.83	9.77	14.65	143.10
Standard Deviation		7987.35	1181.80	14.22	0.69	0.64	0.06	1.21	10.85
Percentage Error,%		13.61	3.60	4.75	3.30	1.21	0.66	8.26	7.58
4	5"-1236	48354.00	31634.00	297.00	20.20	51.70	9.80	12.26	120.15
4	5"-1230	49074.00	33375.00	304.00	21.00	46.10	9.20	13.06	120.15
4	2"-1181	48500.00	34200.00	340.00	21.40	47.80	9.80	13.10	128.38
Average		48642.67	33069.67	313.67	20.87	48.53	9.60	12.81	122.89
Standard Deviation		380.61	1309.97	23.07	0.61	2.87	0.35	0.47	4.75
Percentage Error,%		0.78	3.96	7.36	2.93	5.92	3.61	3.70	3.87
8	5"-1236	49023.00	35123.00	263.00	21.40	38.34	7.50	13.26	99.45
8	5"-1230	47975.00	36830.00	265.00	22.05	39.77	8.60	13.30	114.38
8	2"-1181	46834.00	37829.00	321.00	21.10	37.80	8.40	13.50	113.40
Average		47944.00	36594.00	283.00	21.52	38.64	8.17	13.35	109.08
Standard Deviation		1094.83	1368.35	32.92	0.49	1.02	0.59	0.13	8.35
Percentage Error,%		2.28	3.74	11.63	2.26	2.63	7.17	0.96	7.66

Table 4.3 Results of Measurements using different TEPC counters and different tissue sizes.

Neutron Energy (MeV)	***Sphere Diameter (μm)***	$\bar{y}_F$ ***(keV/μm)***	$\bar{y}_D$ ***(keV/μm)***		***Sphere Diameter (μm)***	$\bar{y}_F$ ***(keV/μm)***	$\bar{y}_D$ ***(keV/μm)***
1.5*	2.0	33.8	57.7		4.0	32.0	47.5
6*	2.0	16	48.3		4.0	-	37.9
Am-Be	2.0	21.0	52.8		4.0	20.8	48.0

*Experimental data published by Srdoc and Marino[13]

Table 4.4 Comparison of Experimental Data for Spherical Diameter of 2 μm and 4 μm obtained in this study with others.

Neutron Energy (MeV)	***Neutron fluence(n.cm^{-2})***	***Neutron detection efficiency (count.cm^2)***	$\bar{y}_F$ ***(keV/μm)***	$\bar{y}_D$ ***(keV/μm)***	$\bar{Q}$
2*	1.6E+6	8.2E-2	35.5 ±3.8	51.2 ± 5.4	14.7 ± 1.6
5*	1.3E+7	1.7E-1	22.2 ±2.4	48.6 ± 5.2	10.6 ± 1.1
Am-Be	1.5E+2	1.1E-1	20.0 ±0.1	50.7 ± 3.3	11.2 ± 0.7

*Experimental data published by Nunomiya et.al[48]

Table 4.5 Comparison of Experimental Data for Spherical Diameter of 3 μm obtained in this study with others.

Taking into account only elastic scattering with hydrogen atoms, the energy deposited by a proton depends on its energy upon entering the sensitive gas and on its trajectory length in the gas. Table 4.6 compares the fraction of some microdosimetric parameters, in 10 keV/µm bins, covering the events of protons interaction with the sensitive gas for the range 10 keV/µm to 130 keV/µm for 2 µm site size under Am-Be neutron field. As shown from the table, some spectroscopic information can be extracted and more than 65% of the deposited energy by recoil protons was due to low lineal energy events from 10-30 keV/µm. A result expected from the stopping power values of the recoil protons at the range of energies of neutrons used in this work.

Lineal Energy keV/µm	Fraction of Energy Deposited,%	$\bar{y}_F$,%	$\bar{y}_D$, %	Fraction of $\bar{Q}$, %	Fraction of absorbed Dose,%
10-20	50.5	53.6	36.4	24.1	27.1
20-30	22.8	11.8	10.5	13.0	20.9
30-40	10.5	8.1	8.5	10.5	13.7
40-50	5.8	6.1	7.5	9.2	9.7
50-60	3.2	4.4	6.1	7.6	6.2
60-70	2.3	3.9	6.0	7.4	6.1
70-80	1.6	3.1	5.4	6.7	4.4
80-90	1.1	2.6	5.1	6.3	3.7
90-100	0.9	2.3	4.7	5.9	3.0
100-110	0.6	2.0	4.4	5.0	2.6
110-120	0.4	1.4	3.4	3.0	1.7
120-130	0.2	0.8	2.0	1.5	1.0

Table 4.6 Fractions of microdosimeteric parameters as function of lineal energy for the 2 µm site size.

Table 4.7 show a comparison between our results with Am-Be neutron source and published measurements of ^{238}Pu-Be[49]. Both have the same average neutron energy but with some differences in the field spectra.

Lineal Energy keV/µm	Am-Be fraction of Energy Deposited,%	Pu-Be fraction of Energy Deposited,%[49]
10-20	50.5	57.7
20-30	22.8	20.5
30-40	10.5	8.9
40-50	5.8	4.8
50-60	3.2	2.7
60-70	2.3	2.0
70-80	1.6	1.4
80-90	1.1	1.2
90-100	0.9	0.5
100-110	0.6	0.2
110-120	0.4	0.1
120-130	0.2	0.05

Table 4.7 Comparison of the fraction of energy deposited as function of lineal energy for Am-Be with Pu-Be for 2µm site size.

The efficiency of the 5" TEPCs used has an average value of about 250 counts per µSv of dose equivalent or equivalently 0.07 counts per second per µSv/hr. For most applications, a range from 10-1000 µSv is required, Thus TEPC are useful as dose equivalent meters but need long irradiation periods. To achieve a sensitivity of conventional dose equivalent meter, i.e. 800 counts per µSv for SNOOPY rem meter[50], a TEPC with a diameter about 23 cm is needed.

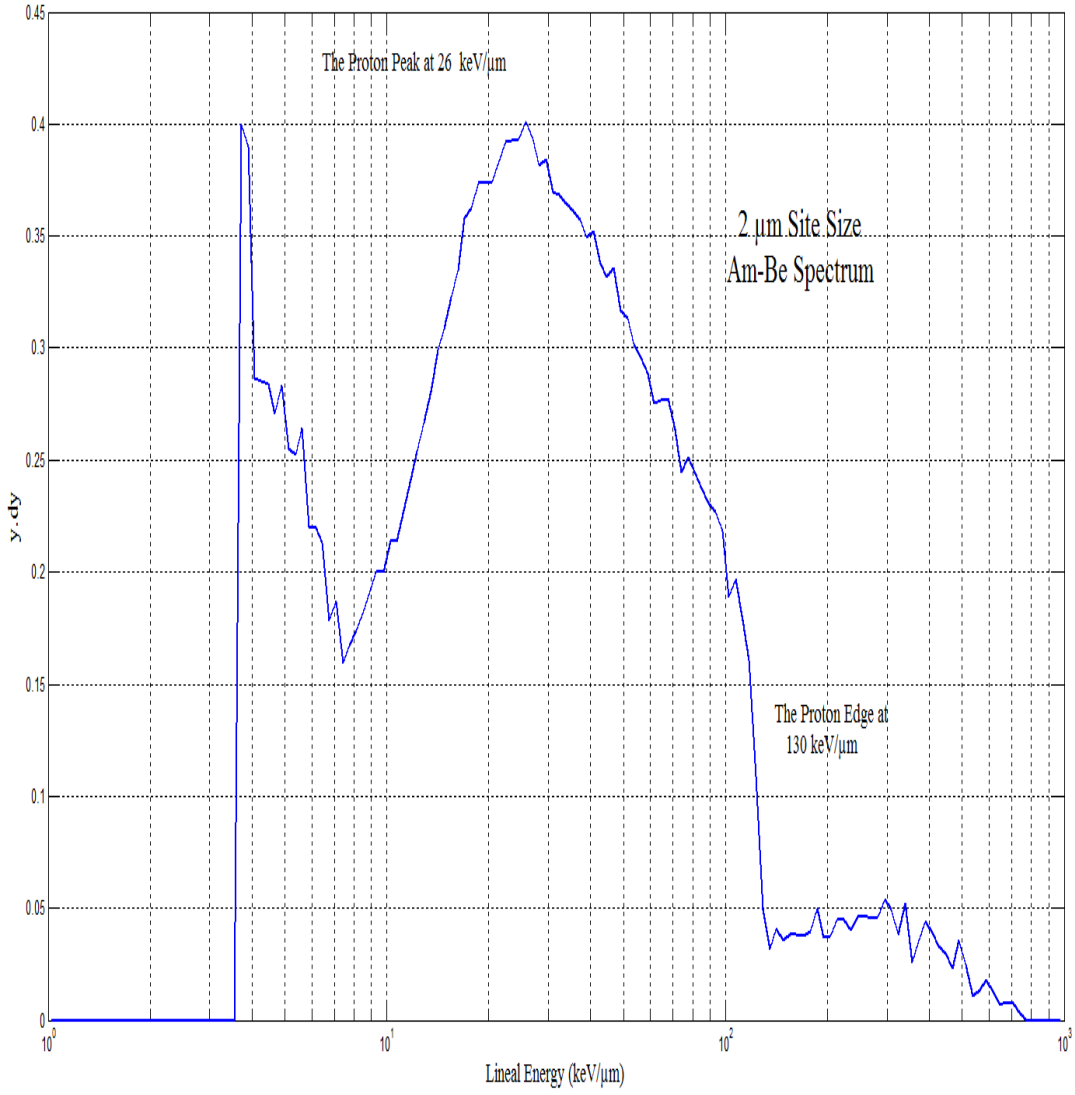

Figure 4. 2 Event-size spectra measured with a TEPC simulating a site size of 2 µm for Am-Be field.

4.1.3 Measurement of Microdosimetric Dose Distribution for Different Neutron Energies :

Neutrons interact with matter in a way that depends to a large extent on their energies and the elemental composition of the absorbing medium. Therefore, the neutron energy has a substantial influence on the shape of the microdosimetric spectra due to different secondary charged particles produced.

The change of the lineal energy spectrum of neutrons with different energy at a given site diameter, d = 2 µm for Am-Be neutrons from this study and compared to the experimental work reported by others[51], is demonstrated in Figure 4.3. Energy, range and LET of the secondary charged particles generated by the Gamma-Neutron fields discuss the most prominent features of these spectra. The predominant interaction mode of fast neutrons with tissue is elastic collisions with hydrogen nuclei. As long as the neutron energy is low enough that the maximum range of the protons is less than the site size, increasing the neutron energy from 0.144 MeV to 0.57 MeV causes the proton peak maximum to extend to higher values of linear energy. Increasing the neutron energy will increase the average proton energy, and hence the amount of deposited energy inside the same site increases leading to a higher linear energy value. When the energy is large enough that the range of protons becomes larger than the site size (above 0.57 MeV), increasing the neutron energy (and hence the average proton energy) causes the proton peak maximum to extend to lower values of lineal energy. This shift in position of the proton peak maximum expresses the fact that with increasing neutron energy the average recoil proton energy will be higher and the average proton stopping power will be lower. This decrease in stopping power will lead to lower values of lineal energy. As the

imparted energy is the integral of the stopping power along the path length, therefore a maximum value 'proton edge' will be obtained for recoil protons that have a residual range that matches the sensitive volume diameter. The stopping power of secondaries as electrons or protons will increase with decreasing energy, the event-size generated by these secondaries in crossing a cavity of size 'X' will depend on both their range and stopping power. Thus for a finite site size 'ΔX', the average stopping power 'ΔE/ΔX' will have a maximum value. This maximum is related to secondaries with ranges that match the cavity size 'ΔX'. As a result for every simulated diameter there is a corresponding maximum ''ΔE/ΔX" for each secondary which represents the location of shoulders for these secondary particles in the event-size spectra. Values of 'y' higher than the shoulder region are caused by those secondary charged particles having higher LET. For a 2 μm simulated site size the lineal energy value of the proton edge is 130 keV/μm for protons and the electron edge is at about 10 keV/μm. Beyond the proton edge at y = 130 keV/μm the contribution of alpha particles and heavy recoil ions of carbon, nitrogen and oxygen is evident and increases in importance with increasing neutron energy.

Referring to the Figure 4.3 It is seen that the y-spectra of 2.5 MeV neutrons and Am-Be neutrons of average energy of 4.5 MeV are similar to each other, except that at 2.5 MeV the (n,α) cross section are just becoming important and so the contribution to the total dose from alpha particle event is still quite small. The peak of the 2.5 MeV neutron spectrum appears at 36 keV/μm at a somewhat higher y-value in comparison to Am-Be neutrons which have a peak at 26 keV/μm, due to the lower average recoil proton energy in the first case. Both spectra present a shoulder at the upper end of the spectrum. In the cases of these two spectra, the mean energy of the protons produced by the neutron

interaction with hydrogen nuclei is around 1.25 MeV for 2.5 MeV neutrons and 2.25 MeV for Am-Be. Protons of these energies will have a range of 35 and 93 μm consequently in unit density tissue, much greater than any of the site diameter of these microdosimetric measurements. It is these so-called 'crosser' protons whose energy deposition is related directly to their LET, which are responsible for the formation of the peak in the event size spectrum and the lower energy protons associated with the 2.5 MeV neutrons produce a "crosser peak" of slightly higher y-value than Am-Be neutrons. As the crossing protons have a range very much more than the site diameters, the position of these peaks for each neutron energy does not depend on the site diameter used for the measurement. The high energy tail begins to split into distinct peaks, belonging to α particles and heavy recoils above 2.5 MeV and become very significant at higher energies, i.e.14.8 MeV neutrons.

Figure 4.3 shows the change in the shape of the spectra with neutron energy for a site size of 2 μm. The 0.57 MeV spectra have a sharp proton cutoff at approximately 130 keV/μm. At higher neutron energies, the recoil proton peak is shifted to lower y values: For Am-Be neutrons the proton peak lies around 26 keV/μm, whereas for 14 MeV neutrons it lies around 10 keV/μm. Neutrons above 1 MeV produce heavy recoils with sufficient energy. A short "tail" belonging to α particles and heavy recoils (C, N, and O) is evident between 130 and 700 keV/μm on the 4.5 MeV spectrum, becoming more prominent as the neutron energy increases.

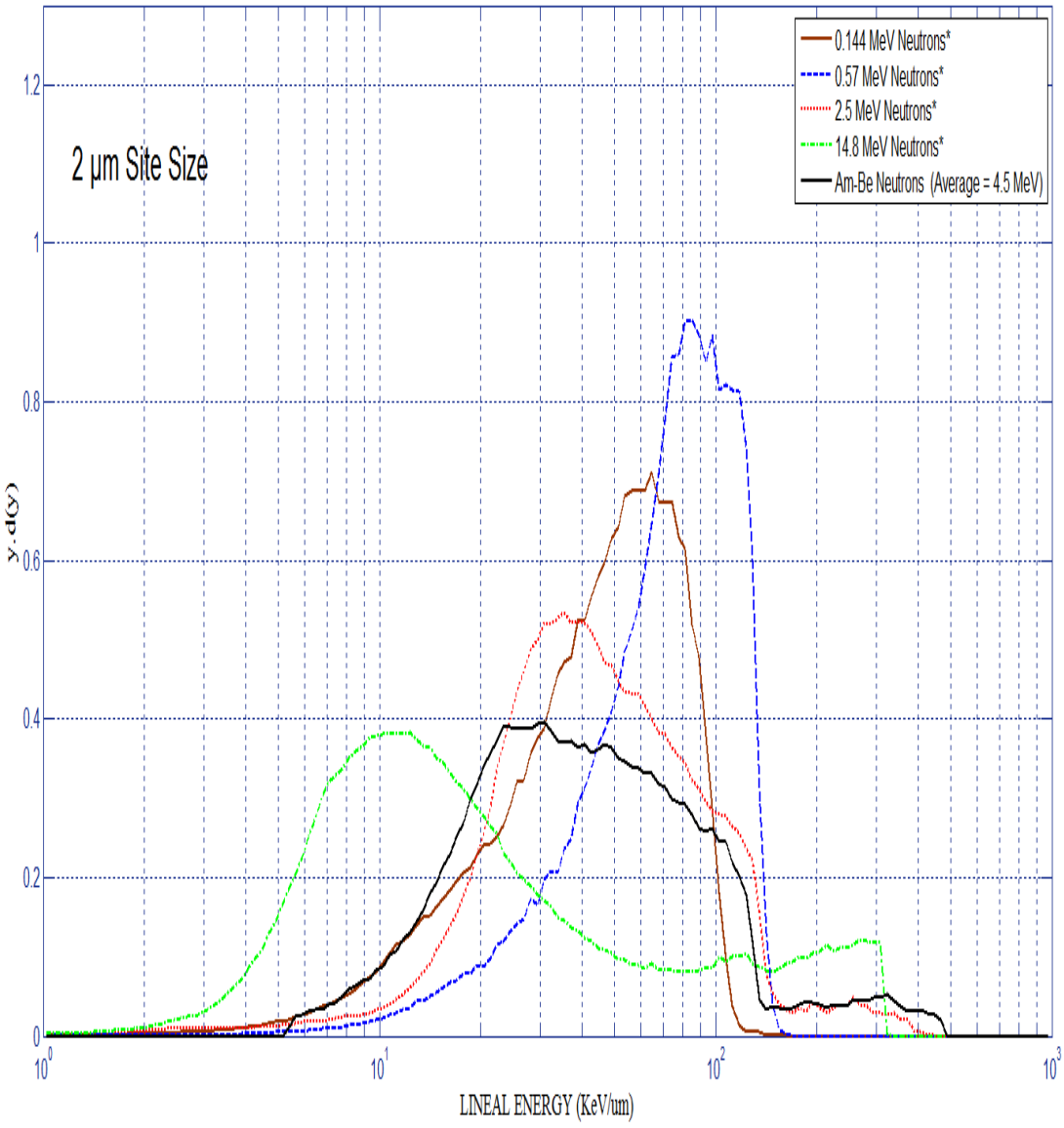

Figure 4.3 The dose fraction per logarithmic interval of lineal energy for different neutron energies. Data denoted by (*) are taken from reference 51.

4.1.4 Measurement of Microdosimetric Dose Distribution for Different Simulated Site Sizes

Another parameter, which has an influence on the shape of the microdosimetric spectra, is the simulated site size. Site size can be changed by changing gas pressure inside the counters.

Figure 4.4 , correspond to the lineal energy y-spectra of Am-be source at 2 µm, 4 µm and 8 µm simulated site diameters respectively. The most significant feature in all these spectra is that, by increasing the simulated site size, the spectra shift to lower lineal energy values accompanied by a narrowing of the spectral distributions. This general behaviour can be explained based on the consideration of secondary charge particles ranges and cavity size as follows: As the cavity size increases, the deposited energy by insider and stopper secondary particles is divided by a larger mean chord length $\bar{l}$, therefore the spectra shifts to lower y-values.

In addition from figure 4.4, it is also observed that for 4 µm and 8 µm, the dose peaks have appeared at higher value of y.d(y), i.e. the spectra have been reduced in width. For Am-Be neutrons, the most prominent interaction for energy transfer is hydrogen scattering. The energies of the initial proton recoil flux, having an approximately rectangular spectrum, intercepted by spheres of different dimensions. Thus inside the cavity as well as in the walls of the counter protons will be generated having a range greater than the mean chord length of a 2 µm diameter simulated site. Therefore the width of the event-size spectrum will be determined by energy loss fluctuations of the protons due to changes in path-length and stopping power. In increasing the site diameter the mean chord length $\bar{l}$ rapidly becomes greater than the range of the protons, thus the event

size spectrum consists of mostly insider and stoppers and fluctuations in energy loss are decreased. Thus the area normalised spectra for 4 μm and 8 μm appear as narrow peaks shifted to lower event sizes. Table 4.8 shows the lineal energy y and deposited energy ΔE in keV at the edge position and at peak for the prominent regions of the event size spectra for the different site sizes.

Simulated Site Diameter (μm)	Mean Chord Length $\bar{l}$ (μm)	Edge Position		Dose Peak	
		y (keV/μm)	ΔE (keV)	y (keV/μm)	ΔE (keV)
2.0	1.33	130	172.9	26	34.6
4.0	2.67	110	293.3	26	69.4
8.0	5.33	98	522.3	18	95.9

Table 4.8 The lineal energy y and the deposited energy (ΔE) values for the prominent regions of the event-size spectra.

As the simulated diameter increases from 2 μm to 4 μm , it is seen that the imparted energy which is calculated from the position of the dose peak is increasing by 34.8 keV. Further increase of site diameter by four times from 2 μm to 8μm will increase the imparted energy by only 61.3 keV. This can be explained by the growing effects of other particle tracks (insider, starter and stopper) over crosser as the site diameter increased. The SRIM code results shows that for energy less than 500 keV, the range of protons in propane based tissue equivalent gas are less than 8μm. As long as the ranges of

the secondary charged particles are less than the simulated site size, there will be an increase in the contribution of starters, stoppers and insiders over the crossers.

One of the prominent features of the spectra shown in figure 4.4 is the presence of some subsidiary peak at y= 75 keV/µm for the 8 µm site size. The deposited energy corresponding to this peak was calculated to be approximately 400 keV. This might be produced due to high energy protons generated by thermal neutron captures by nitrogen nuclei $^{14}N(n,p)^{14}C$. The increase contribution of starters, stoppers and insiders may be a second reason for this peak.

For site size simulated diameter of 8 µm, the maximum proton edge is about 98 keV/µm and the maximum energy deposited by traversing protons is about 522 keV a value which is less than the maximum deposited energy by recoil carbon ions originating and terminating in the gas volume, which is about 1260 keV (0.28*4500keV) . For this reason most of the recoil carbon nuclei energy deposited in the cavity appears in the region above the proton edge.

Table 4.9 show the fraction of energy deposited by recoil proton per 10 keV/µm bins for different site size. The 2µm show more events in the high lineal energy range than the 4µm and 8 µm sizes accompanied with lower fraction of deposited energy by low lineal energy events. This can be explained by the fact that this increase of diameter is not accompanied by more energy deposition, and therefore the whole spectrum is shifted toward lower lineal energy values. Microdosimetric parameters $\bar{y}_F$ and $\bar{y}_D$ for five fixed simulated diameters of 2 µm, 3 µm, 4 µm, 6.5 µm and 8 µm respectively, irradiated individually by Am-Be source show significant changes for $\bar{y}_D$ only, this is shown in table 4.10 and figure 4.5.

Lineal Energy keV/µm	2 µm	4 µm	8 µm
10-20	50.52	52.86	63.44
20-30	22.83	20.77	17.72
30-40	10.52	9.43	7.59
40-50	5.77	5.90	4.37
50-60	3.22	3.81	2.49
60-70	2.32	2.46	1.82
70-80	1.55	1.71	1.42
80-90	1.14	1.22	0.46
90-100	0.85	0.89	0.22
100-110	0.65	0.67	0.17
110-120	0.41	0.19	0.16
120-130	0.21	0.09	0.16

Table 4.9 Fraction of energy deposited as function of lineal energy for Am-Be for 2µm, 4µm and 8µm site sizes.

Site Size (µm)	$\bar{y}_F$	$\bar{y}_D$
8	20.5	38.6
6.5	20.3	40.5
4	20.9	49.5
3	20.8	51.6
2	21.0	52.8

Table 4.10 The changes in the mean values of $\bar{y}_F$ and $\bar{y}_D$ with site size.

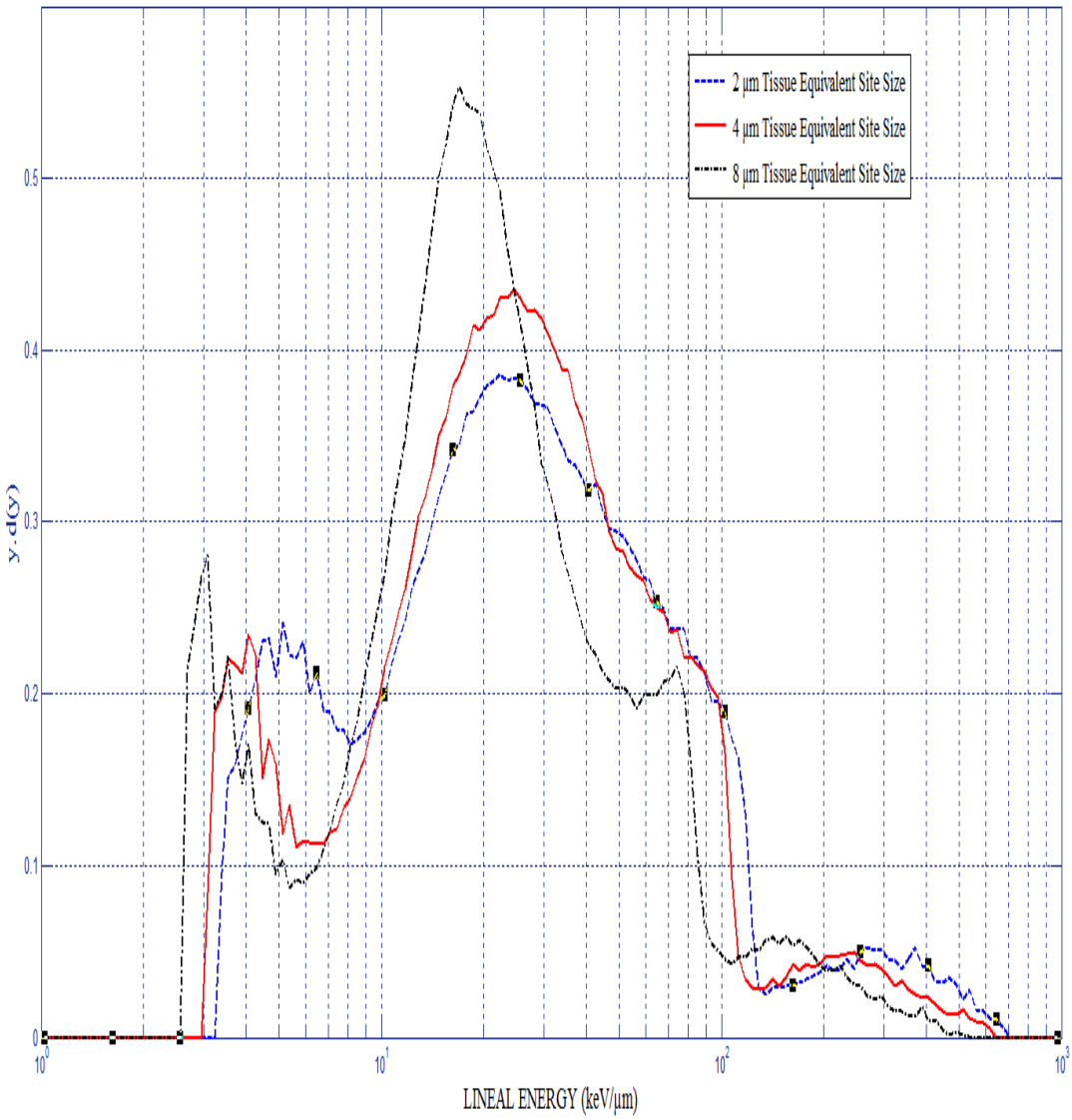

Figure 4.4 y.D(y) distribution for Am-Be source: 2 µm, 4 µm and 8 µm simulated diameters.

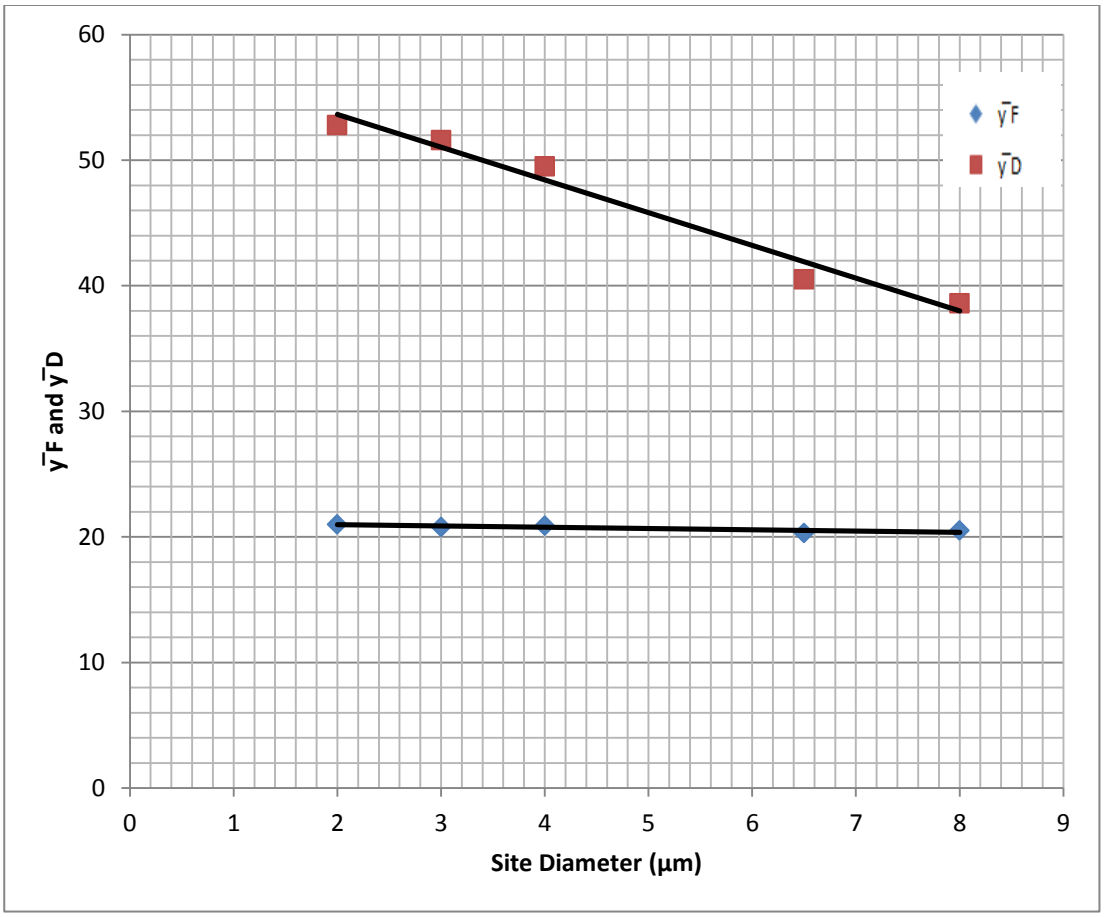

Figure 4.5 The changes in the mean values of $\bar{y}_F$ and $\bar{y}_D$ with site size.

4.2 Determination of the gamma fraction of the total dose

4.2.1 Discrimination by Threshold

For neutron fields with an average energy between 100 keV and a few MeV a distinct minimum is observed in the y-spectra at about 10 keV/µm. This minimum is used to set a threshold in the y spectrum separating neutron and photon dose components. This method can be applied for radiation protection purposes and offers an acceptable accuracy independently of the photon energy. Using this method in this work, the neutron

dose rate is 12.34 μGy/hr and dose equivalent is 111.68 μSv/hr at 13 cm from the centre of the Am-Be source.

4.2.2 Discrimination by Using Gamma Fitting Method

The microdosimetric method of obtaining gamma ray doses or gamma ray dose fractions can be evaluated by the 'fitting' of a pure photon event size spectrum to the appropriate region of the mixed field spectrum. If both the extrapolated mixed field event size spectrum and pure gamma event size spectrum are normalised to unit dose then the fraction of the total dose due to photons is given by the scaling factor required to reduce the pure photon spectrum to superimpose on the lower end of the mixed field spectrum.

For the radiation experiments described in this work, it was proved that most of the photons reaching the proportional counter are 60 keV or degraded gammas coming directly or scattered from the Am-241 part of the neutron source. Figure 4.6 indicates that about 3 mm of lead (Pb) shield is enough to eliminate most of the Am-Be gammas from reaching the proportional counter.

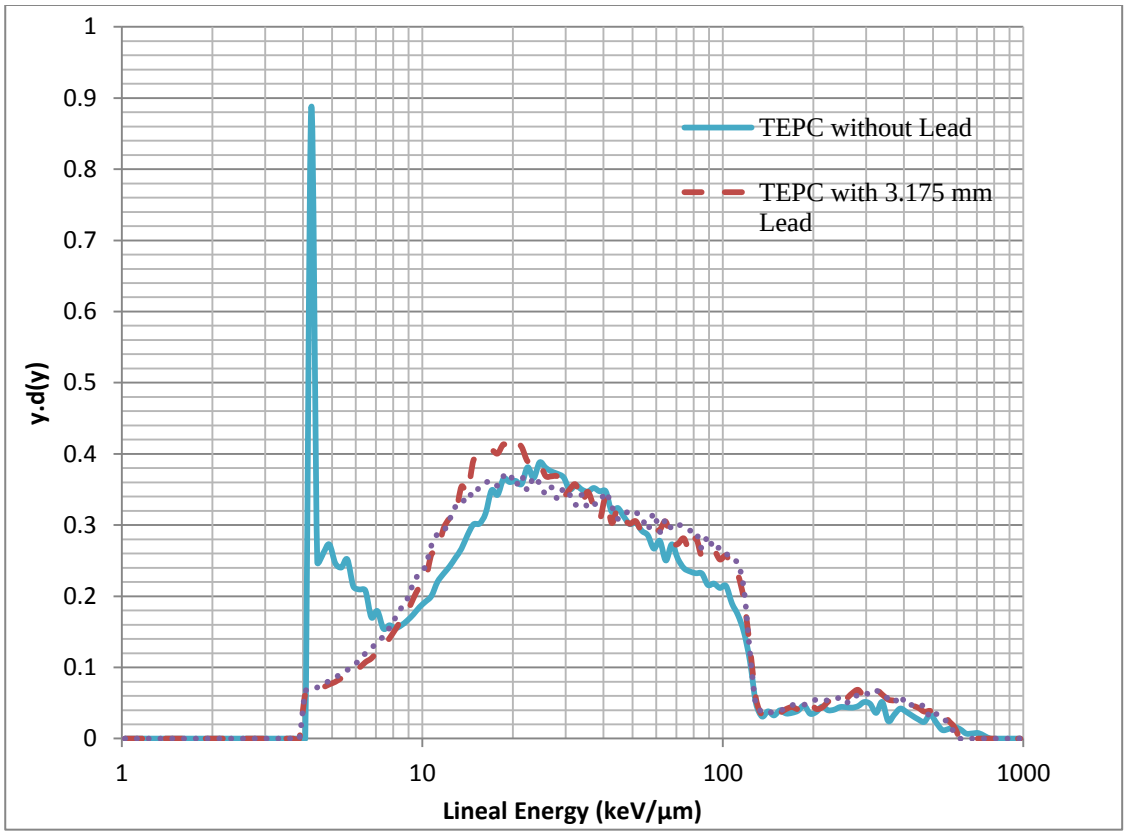

Figure 4.6 The elimination of gammas contribution through using 3.18 & 6.35 mm of Lead shield.

For this reason, ^{241}Am was considered to be a suitable choice for a gamma event size spectrum as well as being the most convenient. Figure 4.7 indicates the quality of the fit between photon and mixed field event sizes. Figure 4.7 (a) shows how the pure normalized ^{241}Am event size spectrum is used to build the extrapolated Am-Be spectrum and the result is shown in step (b). In step (c) of Figure 4.7, the normalized pure ^{241}Am spectrum is scaled down to fit the normalized Am-Be spectrum between the linear energy interval (4 keV/µm to 8 keV/µm). Accordingly, the scaling factor was found to be 2.63, which means that the gamma portion is about 37.9% of the total dose.

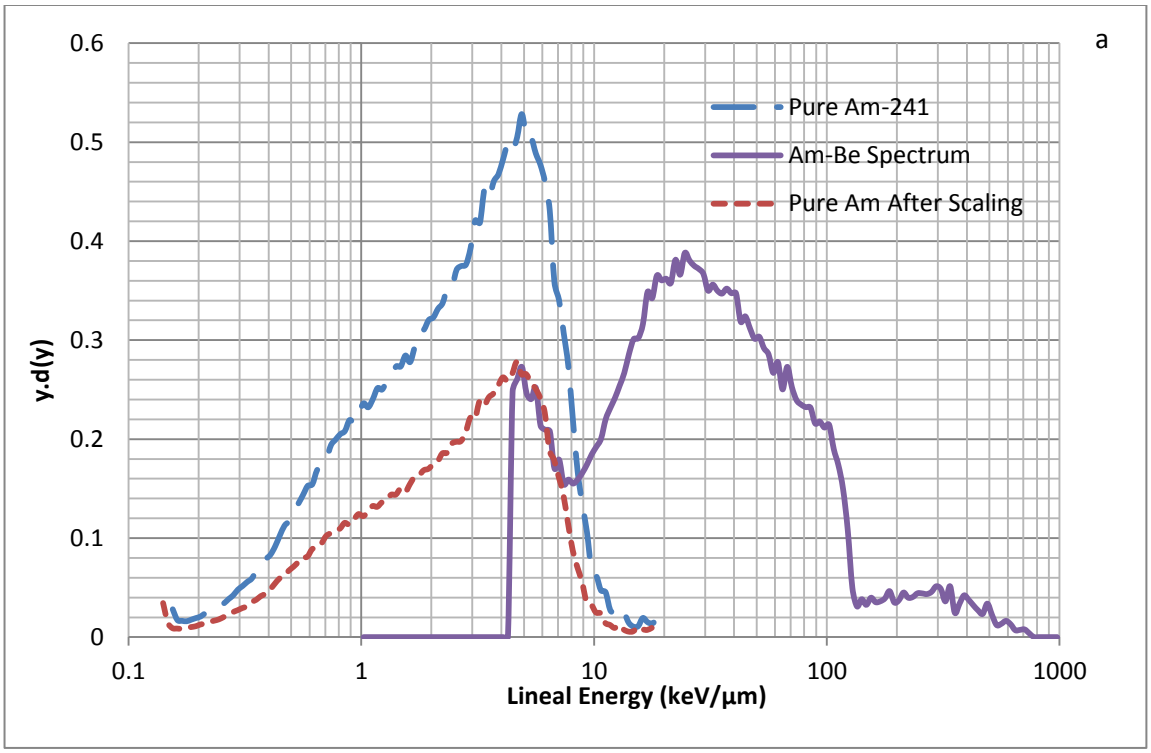
a
0.6
0.5
0.4
0.3
0.2
0.1
0
y.d(y)
0.1
1
10
100
1000
Lineal Energy (keV/µm)
Pure Am-241
Am-Be Spectrum
Pure Am After Scaling

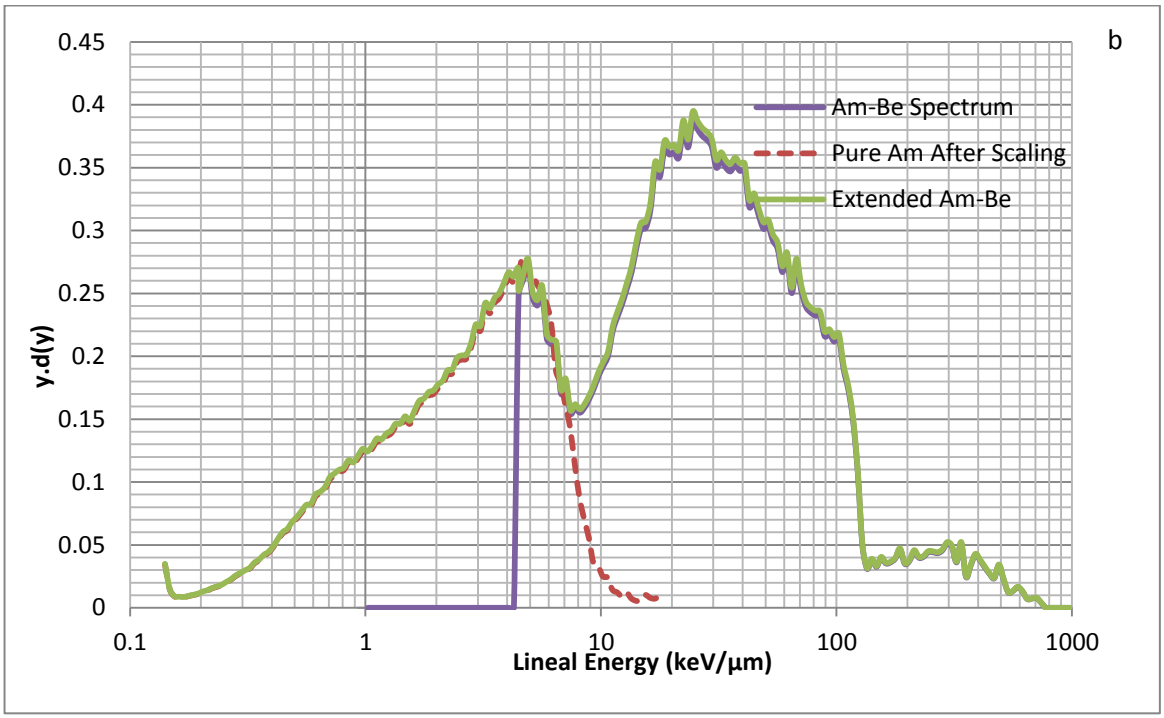
b
0.45
0.4
0.35
0.3
0.25
0.2
0.15
0.1
0.05
0
y.d(y)
0.1
1
10
100
1000
Lineal Energy (keV/µm)
Am-Be Spectrum
Pure Am After Scaling
Extended Am-Be

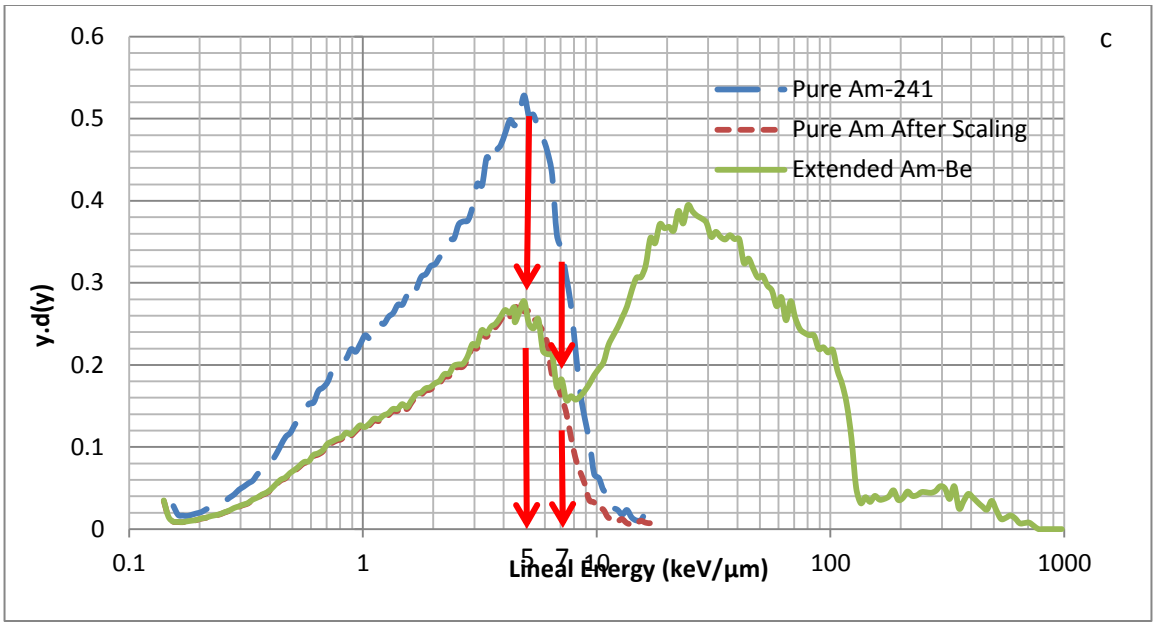

Figure 4.7 (a) The pure ^{241}Am event size spectrum scaled down to fit the lower end of the mixed field spectrum to build the extrapolated Am-Be spectrum to 0.2 keV/µm as shown in step (b). (c) The pure ^{241}Am event size spectrum scaled down to fit the extrapolated mixed field spectrum between the lineal energy interval (4 keV/µm to 8 keV/µm). The scaling factor (2.63) gives the gamma fraction of the total dose.

Generally, by using the gamma fitting method, we note that the photon absorbed dose distribution which contaminates the neutron beam is not identical to the chosen fitting γ rays spectrum. This method of determination of the photon dose may introduce uncertainty due to the appropriateness of the photon distribution being used in the fitting process and the photon energy spectra may not be known well in many photon-neutron mixed fields. Experimental uncertainties in the determination of the photon dose by this method are mainly due to the appropriateness of the photon event size spectrum used and the quality of the extrapolation procedure as well as agreement between the calibration of the two event size spectra[46].

4.2.3 Interrelated Measurements of Tissue Equivalent Plastic Walled counter and a Graphite Walled Proportional Counter

Using detectors with different sensitivity for different radiation components is a common method for separating low-LET and high-LET dose fraction, such as photon and neutrons in mixed fields[25].

The graphite walled proportional counter has two advantages in separating the dose distributions for gamma rays from the distributions measured by using tissue equivalent walled proportional counter, one is the low neutron sensitivity, and another is almost the same sensitivity to gamma rays as the tissue walled proportional counter.

Figure 4.8 (a) shows the dose distributions in the gas cavity of proportional counter, yd(y) as a function of lineal energy ,y , measured with the tissue equivalent-walled (Solid line) and the graphite-walled (Dotted line) counters in a mixed field. In the region of lineal energy from 1 to 15 keV/μm, the photon absorbed dose distribution was measured with the graphite-walled proportional counter by subtracting any proton component; the proton component was subtracted from the photon distribution by fitting and extrapolating the dose distribution between 20-100 keV/μm measured with the graphite-walled proportional counter as shown in figure 4.8 (b) . The photon dose spectrum measured with the tissue equivalent-walled proportional counter is considered to have the same distribution as that measured by the graphite-walled proportional counter, where both have almost the same effective atomic number[24]. Thus, the photon distribution of the tissue equivalent-walled counter was obtained from the scaling down of the pure photon dose distribution measured with the graphite-walled proportional counter, Figure

4.8(c). A scaling factor of 3.2 (i.e., gamma fraction is 31.2%) was used to superimpose both gamma region.

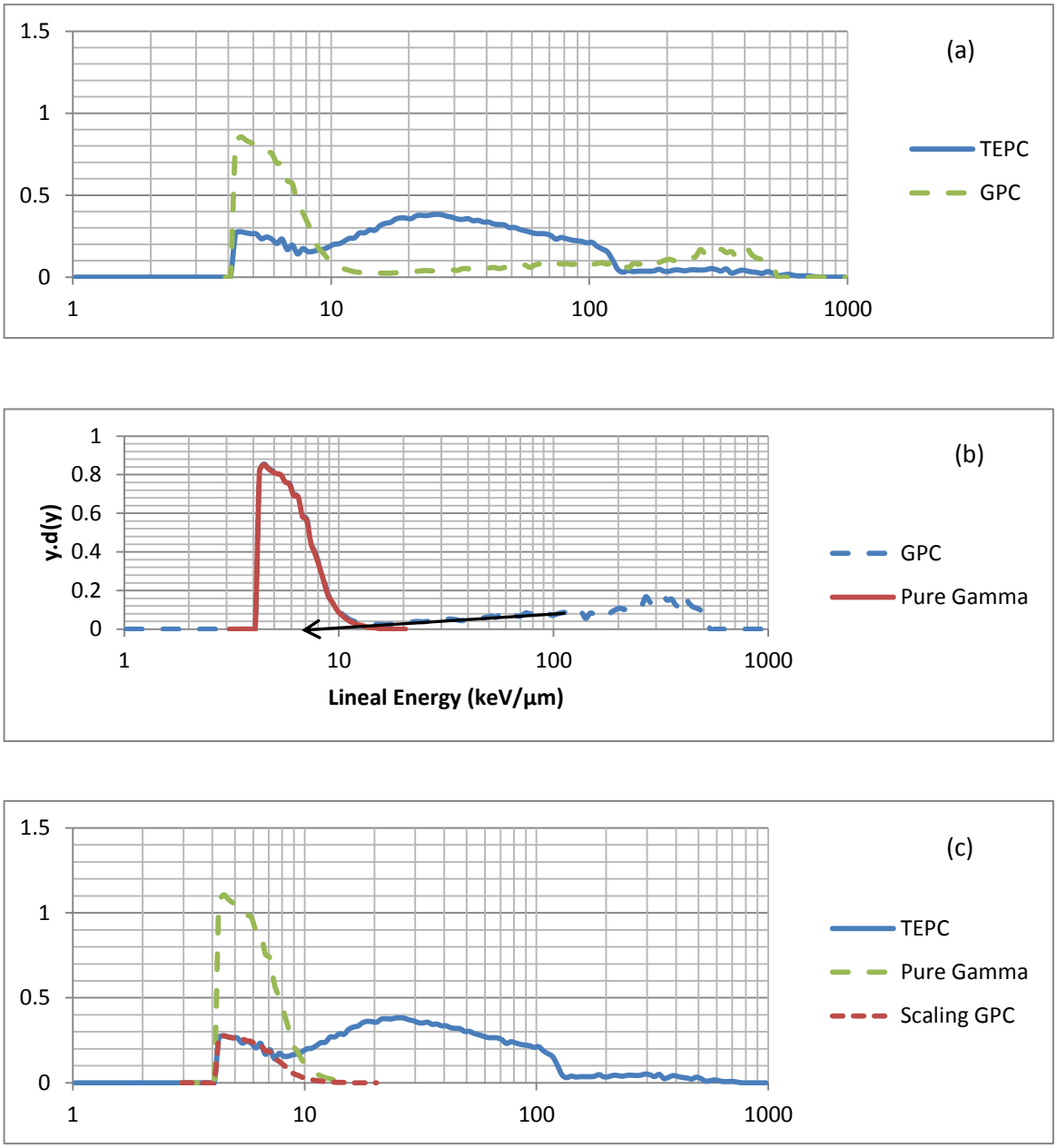

Figure 4.8 (a,b and c) The two detector (TEPC & GPC) technique.

4.3 Discussion of Cavity Theory:

The absorbed dose to a gas cavity is of course determined by the nature of the material surrounding the cavity and the gas cavity itself, this is the essence of cavity theory. By changing the wall material of a proportional counter, valuable information can be obtained.

The Bragg-Gray theory relates the deposited energy to a gas cavity by radiation to the deposited energy in the wall material surrounding the cavity, if charged particle equilibrium is satisfied. In addition the gas cavity inside the medium should not modify the charged particles spectrum which has been created by the wall material surrounding the cavity.

Gray suggested that the ratio of the energy deposited in the medium 'E_m' to that of the gas cavity 'E_g' can be given by the ratio of their stopping powers[9]

$$E_m/E_g = [\ (dE/dX)_{med} / (dE/dX)_g]$$

One of our study objectives was to study the lineal energy spectra measured with both a TEPC & a GPC simulating 2 µm tissue size in the Am-Be field and later to compare it with similar work done by using low-energy neutrons fields[7].

The irradiation of both counters in an Am-Be neutron field, results in events mainly of electrons, protons, alpha particles and heavy ions. The photon dose spectrum measured with the GPC is considered to have the same distribution as that measured by the TEPC, because gamma rays are detected predominately by the Compton scatter within the walls,

and this will depend on the number of electrons available as scattering targets, and both counters have almost the same effective atomic number Z_{eff}.

By using a TEPC, 90% of the distribution in lineal energy range from 10 – 130 keV/ μm is by elastic scattering of neutrons with hydrogen nuclei. The lower lineal energy will be through the overlapped effects of electrons and protons, and above 130 keV/μm by the interactions of alpha particles and recoil nuclei. In GPC, no alpha particles or protons were produced by the neutron interaction with carbon. However, a small number of proton and alpha events are generated in the TE gas. The proton events are produced by hydrogen recoil and by the thermal neutron capture reaction, $^{14}N(n,p)^{14}C$.

Thus, at the microdosimetric level in the neutron energy range we employed in this study, the prevailing events of a GPC filled with TE gas will be recoil carbon from the wall and a very small numbers of protons and α particles from the sensitive gas, while protons are the prevailing events in a standard TEPC's filled with the same gas. Accordingly, the number of events generated in the GPC in the lineal energy range from 10 to 130 keV/μm are of an order of magnitude less than the measured events obtained in the same lineal energy range with a standard TEPC as shown in Figure 4.9.

For GPC irradiated In the Am-Be neutron energy range, we have not observed a lineal energy spectra and microdosimetric averages of a trend similar to that of standard TEPC as it was the case of GPC in low energy neutron fields[7]. This implies that at the microdosimetric level, in Am-Be neutron energy range, the dominant factor which

determines the pattern of the average energy deposited will be the carbon nuclei generated in the counter.

The shape of the dose distributions are predominantly due to alpha particles above 130 keV/µm, are similar when measured with a TEPC or GPC as shown in Figure 4.10, because alpha particles are produced by the same neutron reactions in both counters.

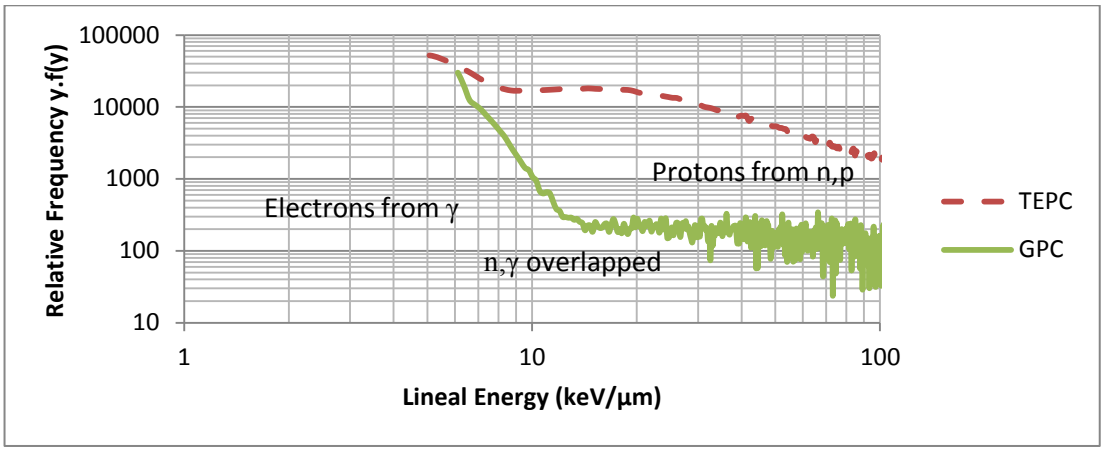

Figure 4.9 The lineal energy spectra measured with TEPC and GPC in the lineal energy range from10-100 keV/µm.

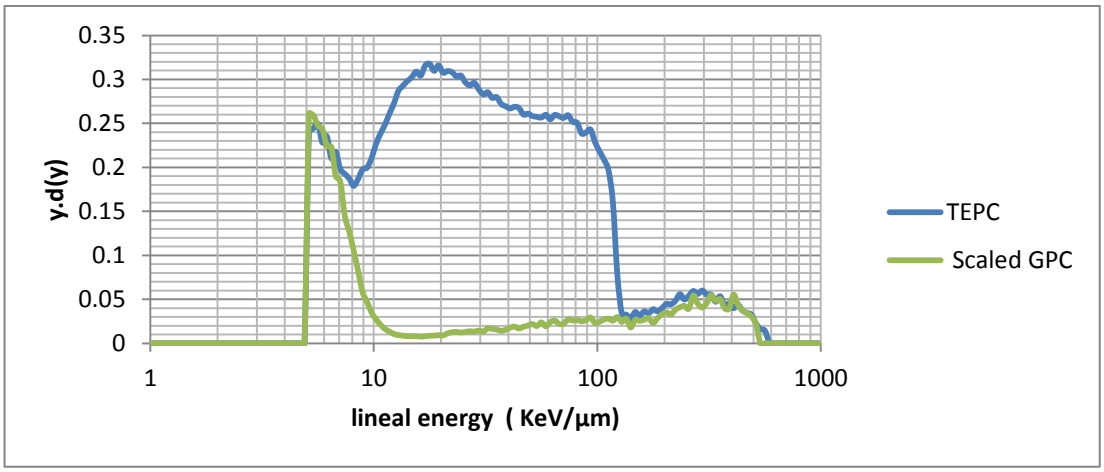

Figure 4.10 Dose distribution measured with Am-Be neutron source by using tissue walled and graphite walled proportional counter

Chapter Five: Conclusion and Future Prospects:

The main objectives of this study was achieved through the determination of the absorbed dose, quality factors, and dose equivalent under mixed neutron gamma field for the UOIT Am-Be neutron source. This study was also aimed at improving the understanding of the underlying physical processes and to investigate the main factors which appears to control the microdosimetric parameters. In an attempt to obtain information for further improving of dosimetry in mixed field environments.

Cavity theory study using different cavity wall is a way to understand the contribution of different secondary charged particle tracks to absorbed dose.

The separation of the gamma dose fraction from the neutron dose fraction is away to characterize the radiation field, as a tool for the determination of dose equivalent where the quality or radiation weighting factors are applied. This was achieved in this study using different techniques. The threshold between low and high LET, the fitting of a previously stored gamma spectrum and the use of detectors with different sensitivity for different radiation components are a common methods for separating low- and high –LET dose fractions.

The objectives were achieved by conducting measurements with TEPCs and GPC at the UOIT neutron facility using Am-Be neutron source.

This chapter provides a discussion of the most important accomplishments presented throughout this thesis and suggests aspects of future research.

5.1 General Conclusions to This Work :

The following conclusion can be drawn from this work:

- Overall uncertainty in the absolute values of microdosimetric parameters has been estimated to be mainly due to counting statistics. The conclusion are supported by the work described in the beginning of chapter four, regarding the assessment of the performance of three proportional counters designed for microdosimetric measurements by measuring the microdosimetric event-size spectra for neutrons produced by the Am-Be reaction under identical radiation field conditions. The three event-size spectra showed good superimposition, and a precision of 3% for the $\bar{y}_F$ and less than 1.3% for the $\bar{y}_D$ and 0.6% for the average quality factor indicates that the energy deposition by all counters are identical. This gives an indication that there are no errors in calibration.
- It was stated in this work that, below 10 keV/µm, most of the events in microdosimetric distribution are due to secondary electrons generating from gamma interactions with the tissue equivalent wall. Through using about 4 mm of lead to shield TEPC, we proved that most of the external gammas were generated of energy less than 60 keV by ^{241}Am. At this photon energies LET of photoelectrons is about 0.6 keV/µm and it will be responsible for the lower event sizes, while most of the recorded large event sizes are due to Compton electrons which have enough energy to deposit most if not all of its energy in the sensitive volume. For the internal gamma in the MeV energy range generated mainly by thermal neutrons capture of hydrogen, the dose belonging to photoelectrons does not have a noticeable effect on the distribution shape, and the role of Compton electrons crossing the site completely in the production of the whole gamma spectrum becomes more and more dominant.

- Taking into account only elastic scattering with hydrogen which is responsible for the main energy deposited in the gas. It is shown in the present study that for neutrons energies of Am-Be source, a significant fraction of protons depositing energy in the gas are of low lineal energy ranged from 10 keV/µm and 30 keV/µm. A result expected from the stopping power values of the recoil protons at the range of energies of neutrons used in this work.
- For Am-Be neutron energy field, it has been observed that $\bar{y}_F$ did not change but $\bar{y}_D$ decreases as the site size increases. The decrease in $\bar{y}_D$ is related to the amount of energy transferred to the cavity by each kind of the particle interaction mechanism. Although, most of the events will be "crossers" which lose energy across the cavity diameter, the amount of energy loss is limited by the size of cavity. Also at the Am-Be neutron energy the three types of event, "starter", "insider", and "stopper" becomes more important and frequently dominant over "crosser", particularly for the heavy particle recoils. As the site size increases, these events will deposit their energy in a distance less than the mean chord length resulting in an underestimate for the microdosimetric parameters.
- The shape of the spectra by using Am-Be neutron source of average energy around 4.5 MeV were compared to other spectra shape of lower and higher energies. As the neutron energy increases, a systematic change in the shape accompanied by decreasing in the mean value of $\bar{y}_F$ and $\bar{y}_D$ were observed. The reason for this is related to the differences in slowing down process. By increasing the neutron energies , a larger number of higher energy secondary charged particles are produced. As the energy of secondary charged particles are increased, its stopping power and LET decreases. This means that for a fixed simulated diameter, the number of crosser or the number of secondary charged particles

contributing to the lower event-size region of the distribution is increased. Thus less energy is deposited and eventually y as well as the mean values of $\bar{y}_F$ and $\bar{y}_D$ are lowered.

- The percentage of the components due to various particles generated in the A-150 tissue equivalent plastic towards the total absorbed dose include the estimated electron component due to photon; proton, alpha particle and recoil nuclei components due to neutrons are summed up in the lineal energy range below 10 keV/ μm, from 10 keV/ μm to 130 keV/ μm, from 130 keV/ μm to 430 keV/ μm and above 430 keV/ μm respectively are 31% electron, 65% proton, 3.5 % alpha particle and 0.5% recoil nuclei. If we cut most of the external gamma by using lead shield the proton percentage of absorbed dose increase to about 89% and alpha particles to 6% and recoil nuclei to 1.1%.
- The neutron detection efficiency, $\in$, represents the number of neutron counts detected by the counter divided by the neutron fluence at the centre position of the counter is about 0.1 counts.cm^2 and fitted well with other experimental data by Nakamura et. al.[48] and well fitted the following simple equation: $\in = 0.045\ E^{0.9}$ where E is neutron energy in MeV. Measured mean quality factors of 9.78 are close to the values given by ICRP-60 and ICRP-74, which is ranged between 9.0-9.5.
- Determination of the gamma and neutron fractions for the Am-Be field in the present work were accomplished through using three techniques. To compare the simple technique which is the discrimination by threshold with the other more sophisticated techniques: Gamma fitting and interrelated measurements of TEPC and GPC we need first to extend the low lineal energy range of our TEPC measurements to cover lineal energies in the 0.1 keV/μm to 3.0 keV/μm. This was done by assuming that the spectra in this region is similar to that produced by pure ^{241}Am. Thus, we find that the gamma

fraction resulted by events less than 10 keV/μm is about 48% of the total absorbed dose. By using gamma fitting technique the fraction of the total dose due to photons was 37.9%, while it is 31.2% By using GPC and TEPC interrelated technique. The degree of error introduced by using a lineal energy threshold compared to the other techniques is about 30%.

5.2 Future Prospects :

The use of TEPCs in radiation spectrometry to describe the intensity of a radiation with respect to energy is an important field of research in radiation protection physics. If the total number of events divided according to their lineal energy into different region, these regions will serve as a spectroscopic tool. TEPC can be used in mixed field spectrometry due to its ability to differentiating between signals from neutrons and photons. The great challenges in workplace neutron spectrometry are the discrimination against the photon components.

Research is required to improve the control on TEPC sensitivity in order to reduce measurement time at low dose rate and prevent pile-up problems at high dose rates. One of the major difficulties with making neutron spectrometry measurements for protection purposes is the very wide range of energies which need to be covered accompanied with the varying response of TEPCs at low and high neutron energies. Changing some design or operating parameters such as wall material, wall thickness, sensitive gas component and pressure may be lead to overcome these difficulties.

Appendix A : MATLAB Code

```
% Purpose of Code: Convert Exprimental Spectrum to yd(y) Microdosimetry
% Spectrum for up to 5 Spectrum
%=========================================================================
===

%Step (1) State Logarithmically-Spaced (Base 10) Lineal Energy Values

h = zeros(151,1);
h(1,1) = 1;

for i=2:1:151
    h(i,1) = 10^((i-1)/50);
end
Ady = zeros(150,1);
Bdy = zeros(150,1);
Cdy = zeros(150,1);
Qdy = zeros(150,1);
Kdy = zeros(150,1);

%Excel spreadsheet must be in directory

for W=1:1:5
if W ==1
ED =xlsread('final');
end
if W==2
ED =xlsread('XXX');
end
if W==3
ED =xlsread('5Inch1230Final');
end
if W==4
ED =xlsread('5Inch1236Final');
end
if W==5
ED =xlsread('XXX');
end
f = zeros(151,1);

for j = 1:1:150
     for k = 2:1:length(ED)
         if (ED(k,1)>=h(j,1) && ED(k,1)<=h(j+1,1))
             f(j+1) = f(j+1) + ED(k,2);
         end
     end
end

nz = zeros(151,1);
z = 0;

for q = 1:1:151
```

```
    if (f(q,1) ~= 0)
        z = z+1;
        nz(z,1) = q;
    end
end
z1 = 0;
z2 = 0;

for r = 1:1:150

    if ((nz(r+1,1)-nz(r,1)) > 1)
        z1 = nz(r+1,1)-nz(r,1);
        z2 = f(nz(r+1,1),1)/z1;
    end

    if (z2 > 0)

        for s = (nz(r,1)+1):1:nz(r+1,1)
            f(s,1) = z2;
        end
    end

    z2 =0;

end

%This is Case-by-Case

%z3 = f(32,1)/5;

%f(28,1)=z3;
%f(29,1)=z3;
%f(30,1)=z3;
%f(31,1)=z3;
%f(32,1)=z3;

y_m = zeros(150,1);

for m=1:1:150
    y_m(m,1) = 0.5*(h(m,1)+h(m+1,1));
end

yfy_t = 0;

for n=1:1:150
    yfy_t = yfy_t + y_m(n,1)*f(n+1,1);
end

ydy = zeros(150,1);

for p=1:1:150
   ydy(p,1) = y_m(p,1)*f(p+1,1)/(yfy_t*0.04605);

    if W==1
```

```
    Cdy(p,1) = ydy(p,1);
    end
    if W == 2
    Bdy(p,1) = ydy(p,1);
    end

    if W == 3
    Ady(p,1) = ydy(p,1);
    end
   if W == 4
    Qdy(p,1) = ydy(p,1);
   end
    if W == 5
    Kdy(p,1) = ydy(p,1);
    end
end

end

semilogx(y_m,Ady,'-y');
hold on
semilogx (y_m,Bdy,'--');
hold on
semilogx (y_m,Cdy,'-r');
hold on
semilogx (y_m,Qdy,'-g');
hold on
semilogx (y_m,Kdy,'-k');
hold off

xlabel('LINEAL ENERGY (KeV/um)')
ylabel('yd(y)')
title('8 Micron Tissue Equivalent')
```

References :

1. Bilski P. et.al "The problems associated with the monitoring of complex workplace radiation fields at European high-energy acclerators and thermonuclear fusion facilities", Radiation Protection Dosimetry, Vol. 126, 2007, , No. 1–4, pp. 491–496.

2. Mitaroff, A. and Silari, M. "The CERN–EU high energy reference field (CERF) facility for dosimetry at commercial flight altitudes and in space". Radiation Protection Dosimetry, Vol. 102, 2002, 7–22.

3. International Commission on Radiological Protection, ICRP Report 60, Annals of the ICRP 21, No.1/3, Pergamon Press, New york, 1991.

4. Stark, M.S., Waker, A.J. and Hunt, J.B., "The determination of fluence to dose equivalent conversion factors for Americium, Beryllium, and Californium sources from Microdosimetric Measurements.", Radiation Protection Dosimetry. Vol.18, 1987, No.3, pp.141-146.

5. Booz, J. , Edward , A.A. and Harrison, K.G. , "Microdosimetric counters in radiation protection.", Radiation Protection Dosimetry, Vol. 9, 1984, No.3.

6. D.T. Goodhead, "Track structure considerations in low dose and low dose rate effects of ionzing radiation", Advance in Radiation Biology, 16, 1992, pp. 7-34.

7. Waker, A. J. and Aslam,"Study of microdosimetric energy deposition patterns in tissue-equivalent medium due to low-energy neutron fields using a Graphite-Walled Proportional Counter", Radiation Research 175, 2011, 806-813.

8. Kellerer, A. M. " Microdosimetry: Reflection on Harald Rossi", Radiation Protection Dosimetry, 99, 2002, pp. 17-22.

9. Waker A.J. "Principles of Experimental Microdosimetry", Radiation Protection Dosimetry, Vol.61, 1995, No.4 pp.297-308.

10. Rossi, H.H., Biavati M.H. and Gross W. "Low Energy Density in Irradiated Tissues", Radiation Research, 15, 1961, pp. 431-439.

11. R.S. Caswell, "Deposition of energy by neutrons in spherical cavities", Radiation Research, 27, 1966, pp. 92-107.

12. P. Colautti, M. Cutaia, M. Makarewicz, H. Schraube, G. Talpo, and G. Tornielli, "Neutron microdosimetry in simulated volumes less than 1 μm in diameter", Radiation Prof. Dosim. 13, 1985, pp. 117-121.

13. Srdoc Dusan and Stephen A. Marino, " Microdosimetry of monoenergetic neutrons", Radiation Research, Vol. 146, Oct. 1996, No.4 pp.466-474.

14. I.A.M. AL-Affan, "A new concept in microdosimetry to evaluate the quality factor for neutrons and photons", Rad. Prof. Dos., 23, 1988, (1-4), pp. 83-86.

15. Booz J., "Development of dose equivalent meters based on Microdosimetric principles", Radiation Environment Biophysics, 23 , 1984, pp. 155-170.

16. Edwards A.A. ,"Low pressure proportional counters in radiation protection: Improving to energy response and sensitivity", Radiation Protection Dosimetry, 29, 1989, (1-2), pp. 109-112.

17. Pihet P., Menzel,H.G., Albert W.G. , Kluge H. " Response of tissue equivalent proportional counters to low and intermediate energy neutrons using modified TE-3He gas mixtures". Radiation Protection Dosimetry, 29, 1989, (1-2), pp. 113-118.

18. Gerdung S., Grillmaier R.R., Lim T., Pihet P., Schuhmacher H. and Segur P. " Performance of TEPC at low pressures: Some attempts to improve their dose equivalent response in the neutron energy range from 10keV to 1 MeV". Radiation Protection Dosimetry, 52, 1994, (1-4), pp. 57-59.

19. ICRU, Microdosimetry, Report 36, International Commission on Radiation Units and Measurements, 1983.

20. Kliauga Paul, "Microdosimetry at middle age: Some old experimental problems and new aspirations", Radiation Research, Vol.124, 1990, No. 1, pp. S5-S15.

21. Menzel et al" Investigation of basic uncertainties in the experimental determination of microdosimetric data" in Proceeding, Eighth Symposium on Microdosimetry pp.1061-1072. Commission of the Europian Communities, Luxembourg, 1982.

22. Verma, M.N. " Calibration of Proportional Counters in Microdosimetry" in Proceeding, Eighth Symposium on Microdosimetry pp.1051-1059. Commission of the Europian Communities, Luxembourg, 1982.

23. Takada M. , Baba M., Yamaguchi H. and Fujitaka K. " Differential absorbed dose distributions in lineal energy for neutrons and gamma rays at the mono-energetic neutron calibration facility", Radiation Protection Dosimetry, Vol.114, 2005, No.4 , pp. 481-490.

24. Takada M. , Yamaguchi H.., Uchihori Y., and Fujitaka K. " Differential dosimetry in neutrons-proton mixed field with low pressure proportional counters", Radiation Protection Dosimetry, Vol.97, 2001, No.3 , pp. 213-222.

25. Kyllonen J. and Lindborg L., "Photon and neutron discrimination using low pressure proportional counters with graphite and A150 walls", Radiation Protection Dosimetry, Vol.125 2007, No.1-4 , pp. 314-317.

26. Rossi and Zaider M. " Microdosimetry and its application" Springer 1996.

27. Kellerer A.M. and Rossi H.H. "The Theory of Dual Radiation Action" , Curr. Top. Radiation Research, Q.8, (1972), 85.

28. Kellerer, A.M. "Theory of wall-effects in microdosimetric measurements", Proceedings of a Symposium on Biophysical Aspects of Radiation Quality, Held by the International Atomic Energy Agency in Lucas Heights, Australia, 8-12 March 1971.

29. Ervin B. Podgorsak, " Radiation physics for medical physicists" , Springer, 1st Edition, 2006.

30. Glenn F. Knoll, "Radiation detection and Measurement", 4th Edition, John Wiley and Sons Inc., 2010.

31. Waker A.J. "Gas gain characteristics of some walled proportional counters used in microdosimetry", Commission of the European Communities, Radiation Protection/Microdosimetry, Proceeding of the Eighth Symposium Germany, 1982, Report EUR 8395.

32. Shonka, F. R. , Rose, J.E. and Failla, G., "Conducting plastic equivalent to tissue, air and polystyrene", Second United Nations International Conference on the Peaceful Uses of Atomic Energy.A/Conf. 15/P/753, 1958.

33. International Commission on Radiation Units and Measurements, ICRU Report 10b, Physical Aspects of Irradiation, 1962.

34. Srdoc, D. "Experimental technique of measurement of microscopic energy distribution in irradiated matter using Rossi counter", Radiation Research, 43, 1970, pp.302-319.

35. Rossi,H.H. and Failla, G.,"Tissue equivalent ionization chambers", Nucleonics, 14, 1965, 2 , p.32.

36. James. F. Ziegler, "SRIM: The stopping and range of ions in matter", < http://www.srim.org > , 2011.

37. Farahmand, M. " A novel tissue-equivalent proportional counter based on a gas electron multiplier" , Delft University Press, The Netherlands, 2004.

38. Waker, A.J., "Principles of experimental microdosimetry", Radiation Protection Dosimetry,Vol.61, 1995, No.4, pp.297-308.

39. "Reference neutron radiations-Characteristics and methods of production", International ISO/DIS Standard 8529-1 EDMS 812014, March 27, 2000.

40. K. W. Geiger and L. Van Der Zwan "Radioactive neutron source spectra from 9Be(α,n) cross section data", Nuclear Instruments and Methods, 131, Oct. 1975, pp. 315-321.

41. Far West Technology, Product. From Far West Technology, Inc.

<http://www.fwt.com/detector/letsw5ds.htm> and < http://www.fwt.com/detector/letsw2ds.htm >.

42. Waker A.J., Aslam , " An experimental study of the microdosimetric response of a graphite walled proportional counter in low energy neutron fields", Nuclear Instruments and Methods in Physics Research A:Accelerators, Spectrometers, Detectors and Associated Equipment, Vol. 652, 2011, Issue 1, pp. 721-725.

43. GloriaM. Spirou, Soo-Hyun Byun, William V. Prestwich " Comparison of three pulse processing systems for microdosimetry", IEEE Transactions on Nuclear Science, VOL. 55, Oct. 2008, No. 5, pp. 2621-2625.

44. manual of DP5: < http://www.amptek.com/dp5soft.html >.

45. S. Gerdung P. Pihet J.E. Grindborg H. Roos U.J. Schrewe H. Schuhmacher, "Operation and Application of TEPCs", Radiation Protection Dosimetry, Volume 61, 1995, Issue 4, pp. 381-404.

46. Anthony J. Waker " Experimental uncertainties in microdosimetric measurements and an examination of the performance of three commercially produced proportional counters"), Nuclear Instrumentation and Methods in Physics Research, A234, 1985, pp.354-360.

47. Olko P., Schmitz Th., Morstint K., Dydejczyk A. Booz J. ," Microdosimetric distribution for photons", Radiation Protection Dosimetry, Vol.29, 1989, No.1/2, pp. 105-108.

48. Nunomiya T., Kim E., Kurosawa T., Taniguchi S., Nakamura T., Nakane Y., Sakamoto Y., Tanaka S.,"Measurement of lineal-energy distributions for neutrons of 8 keV to 65 MeV by using a tissue-equivalent proportional counter", Radiation Protection Dosimetry, Vol.102, 2002, No.1, pp. 49-59.

49. Eisen Y., Vasilik D.G., Brake R.J., Erkkila B. H., Littlejohn G. J., "The performance of low pressure tissue equivalent chambers and a new method for parameterizing the dose equivalent", Los Alamos National Labrotary LA-10770-MS, 1986.

50. Tessler G., Glickstien S. S., "Monte-Carlo calculations of the response of the portable neutron monitor SNOOPY", Health Physics, 10, 1975, pp.197.

51. Waker A. J. , Personnal Communication; Experimental data as the investigation that reported: H.G. Menzel, L.Lindborg, Th. Schmitz, H. Schumacher and A.J. Waker "Intercomparison of dose equivalent meters based on microdosimetric techniques: detailed analysis and conclusions", Radiation Protection Dosimetry, Vol.29 1989, No.1/2 pp. 55-68.